PATENT
Attorney Docket No.: 3875-4138US1

IN THE UNITED STATES PATENT AND TRADEMARK OFFICE

In re application of: David McKinnon and Jane Dixon Application No.: 09/786,108 Filed: June 18, 2001 For: Mammalian ELK Potassium Channel Genes	Confirmation No. 6832 Examiner: PAK, Michael D. Technology Center/Art Unit: 1646 DECLARATION UNDER 37 C.F.R. §1.132 OF DR. KRAFTE

Commissioner for Patents
P.O. Box 1450
Alexandria, VA 22313-1450

Sir:

I, Douglas Krafte, being duly warned that willful false statements and the like are punishable by fine or imprisonment or both (18 U.S.C. § 1001), and may jeopardize the validity of the patent application or any patent issuing thereon, state and declare as follows:

1. All statements herein made of my own knowledge are true, and statements made on information or belief are believed to be true and correct.

2. I received a B.S. degree in Molecular Biology from Vanderbilt University in 1981 and a Ph.D. in Physiology from the University of Rochester in 1985. I served as a postdoctoral fellow in the Molecular Neurobiology Section of the Biology Division at The California Institute of Technology from 1985-89. I was a scientist at Sterling Winthrop Pharmaceuticals Research Division from 1989-1994 with titles ranging from Research Biologist to Principal Research Investigator, a Principal Scientist/Sr. Principal Scientist at Boehringer Ingelheim Pharmaceuticals Inc. from 1994-1997, a Principal Scientist/Group Leader at Aurora

Biosciences Corp. from 1997-1999, and Director/Vice President at Icagen from 1999 to the present.

3. The invention of the above-referenced patent application provides for the first time nucleic acids encoding rat elk1, rat elk2 and rat eag2 genes, all of which are expressed in the neuronal ganglia and the nervous system.

4. I have read and am familiar with the contents of this patent application. In addition, I have read the Office Action, mailed September 30, 2004, received in the present case. It is my understanding that the Examiner does not believe that the present invention is supported by a specific, substantial, and credible asserted utility or a well-established utility as required by the United States patent laws.

5. This declaration is provided to demonstrate that the identification of the coding sequences for rat elk1, rat elk2, and rat eag2 has a specific and substantial utility that is credible to one of ordinary skill in the art.

6. The biophysical properties of elk channels are described in detail in Figures 4A-4H of the application and illustrate the kinetics, the voltage-dependence of channel gating, and the pH dependence of these channels. To one of ordinary skill in the area of ion channel biophysical training, as would be attained through normal graduate level education, these properties along with the distribution of the channel allow very accurate estimation of the role these channels play in regulating action potential firing and, therefore, CNS function (e.g., Wang et al. (1998) Science 282: 1794-1795; Sangameswaran et al. (1996) J. Bio. Chem., 271: 5953-5956). From the perspective of an ion channel expert, this level of detail is greater than that provided by gene sequence information for a new enzyme such as a protease, ligase, telomerase, etc. The Examiner has noted that in these latter cases the assignment of a new protein to the family is sufficient to convey a specific, substantial and credible utility. It is my opinion that the level of detail described in the application provides the same or greater level of support for a specific, substantial and credible utility.

7. The utility of the elk and eag channels as tools to define pharmacological selectivity of therapeutic agents is also demonstrated in Figures 4G and 4H where a compound which blocks erg channels, E4031, does not block elk1 channels. Erg channels are related to elk and eag channels (see Fig.1) and yet E4031 does not block elk channels. These specific elk channels are, therefore, very useful in a drug discovery environment to help define selective interactions of drug candidates with different ion channels. In my opinion, this represents a clear real world utility and is consistent with a modern approach to drug discovery.

8. The Examiner has noted that there is no direct link described in the application to show that changes in expression levels of these channels are tied to a given disease. There are many examples, however, where this information is not necessary to identify therapeutically useful agents. Local anesthetics are excellent examples where an acute block of sodium channel activity is therapeutically beneficial even though there are clearly no changes in channel expression following acute injury. The knowledge of the biophysical function and the tissue distribution of the channels is sufficient to predict the therapeutic utility of Na channel blockers. In fact, cloned channels have been utilized to define the interaction of certain classes of drugs with Na channels (e.g., Ragsdale et al. (1991) Mol. Pharmacol. 40: 756-765). This is the same level of information provided in this application for elk/eag channels.

9. The Examiner has also correctly noted that the native configuration of elk or eag channels may include other gene products not necessarily disclosed in the current application. This possibility was discussed in the body of the application as well. While I certainly agree that this is a possibility, there are numerous examples of single gene products being used effectively in the ion channel field to identify novel potential drug candidates. Again, sodium channels are a good example, where the native conformation of the channel includes various beta subunits. However, single subunits can be used effectively to identify agents, which are also active on the native channels. In fact, cloned channels without accessory subunits have been utilized to define the binding site of certain classes of drugs (e.g., Ragsdale et al. (1994) Science, 265: 1724-1728).

10. In my opinion the above scientific arguments indicate that one of normal skill in the art of ion channel biophysics and drug discovery would have found the inventions described in this application useful and valuable at the time the application was filed. One would draw the same conclusion today. The combination of functional characterization, tissue expression and demonstration of unique pharmacological properties within the gene family serve to illustrate this point.

Date: April 4, 2005

By: _____
Douglas Krafte, Ph.D.

References:

Wang HS, Pan Z, Shi W, Brown BS, Wymore RS, Cohen IS, Dixon JE, McKinnon D (1998) KNCQ2 and KCNQ3 potassium channel subunits: molecular correlates of the M-channel. Science 282: 1794-1795.

Sangameswaran L, Delgado SG , Fish LM, Koch BD, Jakeman LB, Stewart GR, Sze P, Hunter JC, Eglen RM, Herman RC (1996) Structure and function of a novel voltage-gated, tetrodotoxin-resistant sodium channel specific to sensory neurons. J. Biol. Chem. 271: 5953-5956.

Ragsdale DS, Scheuer T, Catterall WA (1991) Frequency and voltage-dependent inhibition of type IIA Na channels, expressed in a mammalian cell line, by local anesthetic, antiarrhythmic, and anticonvulsant drugs. Mol. Pharmacol. 40: 756-765.

Ragsdale DS, McPhee JC, Scheuer T, Catterall WA (1994) Molecular determinants of state-dependent block of Na channels by local anesthetics. Science 265: 1724-1728.

THE JOURNAL OF BIOLOGICAL CHEMISTRY
Vol. 271, No. 11, Issue of March 15, pp. 5953–5956, 1996

Communication

Structure and Function of a Novel Voltage-gated, Tetrodotoxin-resistant Sodium Channel Specific to Sensory Neurons*

(Received for publication, December 26, 1995)

Lakshmi Sangameswaran‡, Stephen G. Delgado, Linda M. Fish, Bruce D. Koch, Lyn B. Jakeman§, Gregory R. Stewart, Ping Sze, John C. Hunter, Richard M. Eglen, and Ronald C. Herman

From the Institute of Pharmacology, Neurobiology Unit, Roche Bioscience, Palo Alto, California 94304

Small neurons of the dorsal root ganglia (DRG) are known to play an important role in nociceptive mechanisms. These neurons express two types of sodium current, which differ in their inactivation kinetics and sensitivity to tetrodotoxin. Here, we report the cloning of the α-subunit of a novel, voltage-gated sodium channel (PN3) from rat DRG. Functional expression in *Xenopus* oocytes showed that PN3 is a voltage-gated sodium channel with a depolarized activation potential, slow inactivation kinetics, and resistance to high concentrations of tetrodotoxin. *In situ* hybridization to rat DRG indicated that PN3 is expressed primarily in small sensory neurons of the peripheral nervous system.

Voltage-gated sodium channels play a fundamental role in the regulation of neuronal excitability. In addition to differences in primary structure and kinetic properties (1), these channels can be distinguished pharmacologically on the basis of their relative sensitivity to the neurotoxin, tetrodotoxin (TTX)[1] (2). Two types of sodium currents are expressed by sensory neurons within the dorsal root ganglion (DRG), a fast inactivating TTX-sensitive current and a slow inactivating, TTX-resistant current that appears to be expressed by a high proportion of the small afferent neurons (3–8). Of the large and small neurons of the DRG, the latter is of primary importance in the processing of nociceptive information within the somatosensory system (9, 10). In order to define the molecular basis of sodium channel conductance in sensory neurons, we have attempted to identify and clone novel sodium channel α-subunits. As described here, this work has led to the isolation and functional expression of PN3, a novel voltage-gated, TTX-resistant sodium channel expressed predominantly by small sensory neurons within the peripheral nervous system.

* The costs of publication of this article were defrayed in part by the payment of page charges. This article must therefore be hereby marked "*advertisement*" in accordance with 18 U.S.C. Section 1734 solely to indicate this fact.

‡ To whom correspondence should be addressed: Inst. of Pharmacology, Neurobiology Unit, Roche Bioscience, 3401 Hillview Ave., Mailstop R6E-6, Palo Alto, CA 94304. Tel.: 415-354-2098; Fax: 415-354-7363.

§ Present address: Dept. of Physiology, 302 Hamilton Hall, Ohio State University, 1645 Neil Ave., Columbus, OH 43210.

[1] The abbreviations used are: TTX, tetrodotoxin; DRG, dorsal root ganglion; PCR, polymerase chain reaction; RT, reverse transcription; SCNβ1, sodium channel β1-subunit; h, human; r, rat.

EXPERIMENTAL PROCEDURES

cDNA Cloning—*Eco*RI-adapted cDNA was prepared from normal adult male Sprague-Dawley rat DRG poly(A)$^+$ RNA using the SuperScript Choice System (Life Technologies, Inc.). cDNA (>4 kilobases) was selected by sucrose gradient fractionation (11) ligated into the Zap Express vector (Stratagene) and packaged with the Gigapack II XL lambda packaging extract (Stratagene). Phage (3.5×10^5) were screened by filter hybridization with a ^{32}P-labeled probe (bases 4637–5868 of rBIIa) (12). Filters were hybridized in 50% formamide, 5 × saline/sodium/phosphate/EDTA, 5 × Denhardt's solution, 0.5% SDS, 250 μg/ml salmon sperm DNA, and 50 mM sodium phosphate at 42 °C and washed in 0.5 × SSC, 0.1% SDS at 50 °C. Positive clones were excised *in vivo* into pBK-CMV using the ExAssist/XLOLR system (Stratagene). Southern blots of *Eco*RI-digested plasmids were hybridized with a ^{32}P-labeled DNA probe representing a novel domain IV segment amplified from DRG RNA by PCR with degenerate oligonucleotide primers. Southern filters were hybridized in 50% formamide, 6 × SSC, 5 × Denhardt's solution, 0.5% SDS, and 100 μg/ml salmon sperm DNA at 42 °C and were washed in 0.1 × SSC, 0.1% SDS at 65 °C. A cDNA clone, 7.3, containing a full-length insert, was identified and sequenced on both strands. In addition, several other PN3 clones were partially sequenced. Sequence analyses were done using the Gap, BestFit, PileUp, and Distances programs of the Wisconsin Sequence Analysis Package (Genetics Computer Group, Inc.). For oocyte expression analysis, the PN3 cDNA was excised from the vector and, after blunting the ends, subcloned into pBSTA.

RT-PCR Analysis—Tissues were isolated from anesthetized, normal adult male Sprague-Dawley rats and were immediately frozen at −80 °C. RNA was isolated from tissue samples using RNAzol (Tel-Test, Inc.). Random-primed cDNA was reverse-transcribed from 500 ng of RNA from each tissue. PCR primers targeted the 3′-untranslated region of PN3 and defined a 410-base pair amplicon. Thermal cycler parameters were: 30 s/94 °C, 30 s/57 °C, 1 min/72 °C (24 cycles); 30 s/94 °C, 30 s/57 °C, 5 min/72 °C (1 cycle). A positive control (1 ng of pBK-CMV/PN3) and a no-template control were also included. cDNA from each tissue was also PCR amplified using primers specific for glyceraldehyde-3-phosphate dehydrogenase (13) to demonstrate template viability. PN3 PCR amplicons from nodose ganglia and sciatic nerve were confirmed by nucleotide sequence analysis.

In Situ Hybridization Histochemistry—Oligonucleotide probe sequences were synthesized from the unique 3′-untranslated region of PN3 (sense and antisense probes were complementary to each other). Normal rats were perfused with 4% paraformaldehyde; L4-L5 DRG were removed, postfixed in the same solution, and cryoprotected in 20% sucrose. Frozen sections (10 μm) were cut and hybridized overnight at 39 °C in a solution containing ^{35}S-ATP-labeled oligonucleotides (specific activity, 5×10^7–1×10^8 cpm/μg), 50% formamide, 4 × SSC, 0.5 mg/ml salmon sperm DNA, and 1 × Denhardt's solution. Sections were washed over a period of 6 h in 2 ×–0.1 × SSC containing 0.1% β-mercaptoethanol, dehydrated in a series of ethanols (50–100%) containing 0.3 M ammonium acetate, and apposed to sheet film (Amersham B_{max}) or dipped in liquid emulsion (Amersham LM-1) and then developed for 2 and 5 weeks, respectively. The cell area of neurons (hybridized and non-hybridized) with a distinct nucleolus was measured from sections through the lumbar ganglia with the aid of a Macintosh Quadra 840 using the public domain NIH Image Program (W. Rasband, NIH).

Oocyte Recording—Capped cRNA was prepared from the linearized plasmid using a T7 *in vitro* transcription kit (Ambion, mMessage mMachine) and injected into stage V and VI *Xenopus* oocytes (14) using a Nanojector (Drummond). After 2.5 days at 20 °C, oocytes were impaled with agarose-cushion electrodes (0.3–0.8 megaohm) (15) and voltage-clamped with a Geneclamp 500 amplifier (Axon Instruments) in TEV (two-electrode voltage clamp) mode. Stimulation and recording were controlled by a computer running pClamp (Axon Instruments). Oocytes were perfused with a solution containing (in mM): 81 NaCl, 2 KCl, 1 $MgCl_2$, 0.3 $CaCl_2$, 20 Hepes-NaOH (pH 7.5). The data in Fig. 5*A* were collected using the Geneclamp hardware leak subtraction, filtered at 5 kHz with a 4-pole Bessel filter, and sampled at 50 kHz. For the experiment in Fig. 5*C*, the oocytes were depolarized from −100 mV to +20 mV for approximately 10 ms at 0.1 Hz; P/−4 leak subtraction was used

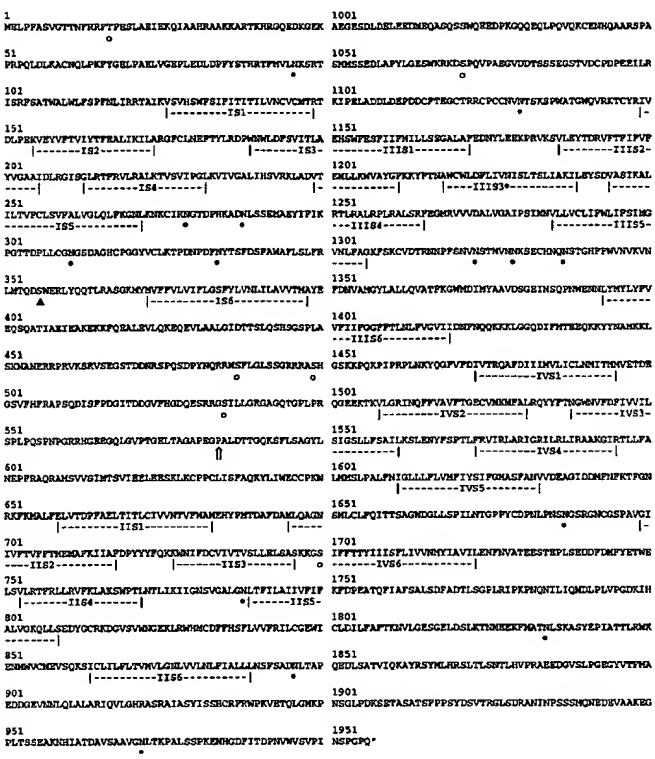

FIG. 1. **Deduced amino acid sequence of peripheral nerve sodium channel type 3 (PN3) showing putative transmembrane domains.** O, potential cAMP-dependent phosphorylation site; ●, potential *N*-linked glycosylation site; ▲, TTX resistance site; *, termination codon; ⇑, site of an additional Gln insertion.

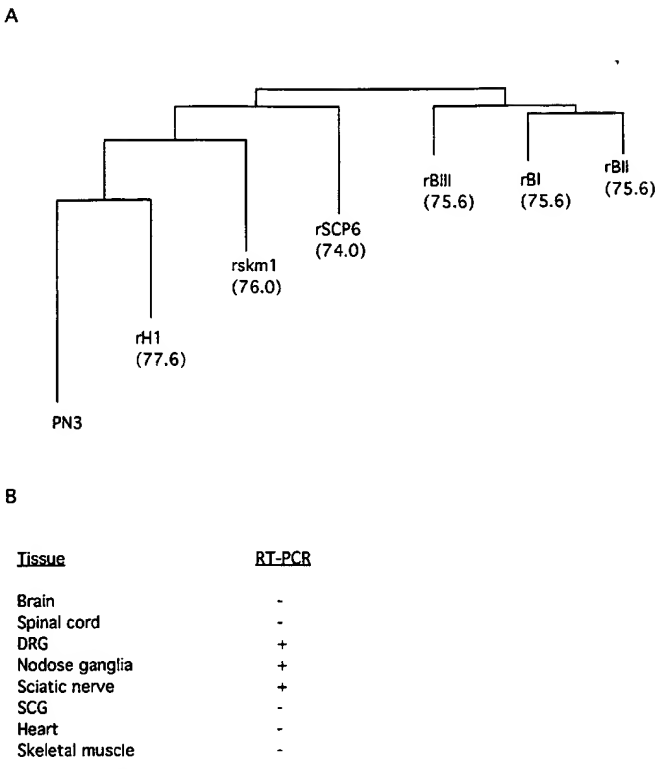

Tissue	RT-PCR
Brain	-
Spinal cord	-
DRG	+
Nodose ganglia	+
Sciatic nerve	+
SCG	-
Heart	-
Skeletal muscle	-

FIG. 2. *A*, amino acid homology comparison of PN3 with selected sodium channels. *Numbers* indicate percent amino acid similarity between each channel and PN3. *B*, tissue distribution profile of PN3 by RT-PCR analysis after 35 cycles of amplification. *SCG*, superior cervical ganglia.

(16). There was a slow "rundown" of the current with time, and a correction was made for the resulting sloping baseline. Varying concentrations of TTX (Sigma) in bath solution were perfused over the oocyte, and the current amplitude was allowed to attain steady state before the effect was recorded.

RESULTS AND DISCUSSION

Sequence Analysis of PN3—To identify novel sodium channel α-subunits from the peripheral nervous system, we used degenerate oligonucleotide-primed RT-PCR analysis of RNA from rat DRG and homology cloning from a rat DRG cDNA library. PCR fragments from domain I and interdomain I–II were cloned and sequenced. The sequences matched those of clones 7.3 and 17.2 that were isolated from the rat DRG cDNA library by homology cloning. Clone 7.3 (PN3, peripheral nerve sodium channel 3) was sequenced entirely. Several other full-length and partial clones for PN3 were isolated.

Nucleotide sequence analysis of the PN3 cDNA identified a 5868-base open reading frame, coding for a 1956-amino acid protein. In common with other sodium channels, there is an ATG 5 base pairs upstream of the genuine ATG. The deduced amino acid sequence of PN3 (Fig. 1) exhibited the primary structural features of an α-subunit of a voltage-gated sodium channel. PN3 contains four homologous domains (I–IV), each consisting of six putative α-helical transmembrane segments (S1–S6). The positively charged residues in the voltage sensor (S4 segments) and the inactivation gate between IIIS6 and IVS1 are highly conserved in PN3; sites for cAMP-dependent phosphorylation and *N*-linked glycosylation shown to exist in other sodium channels (1) are also present in PN3. In PN3, however, there are two unique consensus sites for cAMP-dependent phosphorylation sites, one in domain II between S3 and S4 and another in the interdomain II–III (Fig. 1). Modulation of rBIIa channel function by cAMP-dependent protein kinase A has been demonstrated (1, 17, 18). The significance of the unique cAMP-dependent protein kinase A consensus sites in PN3 *in vitro* and *in vivo* remains to be demonstrated. In addition, there is an insertion of an additional Gln between Pro^{583} and Ala^{584} in several partial clones. The significance of the glutamine insertion has not been determined.

Fig. 2*A* shows an amino acid homology comparison of PN3 with other cloned rat sodium channels. The higher sequence homology between PN3 and the TTX-insensitive cardiac channel and their slow inactivation kinetics (discussed below) suggest that they belong to a unique subfamily of sodium channels. Indeed, the Distance paradigm of the GCG program classifies PN3 and the cardiac sodium channel as a subfamily of sodium channels (Fig. 2*A*).

Other Sodium Channels Isolated from the DRG cDNA Library—In addition to PN3, partial clones for the following known sodium channels were isolated: rBI, rBIII, glial channel (19), and a rat ortholog of the human and mouse atypical sodium channels (20, 21). A β1-subunit was also cloned from the rat DRG by PCR. The rat DRG β1-subunit and rat brain sodium channel β1-subunit (rSCNβ1) have identical amino acid sequences. Human sodium channel β1-subunit (hSCNβ1) and rSCNβ1 (22) are 96% identical.

Expression of PN3—Northern blot analysis using the RT-PCR fragments and the 3′-untranslated region of clone 7.3 as probes showed that PN3 is encoded by a 7.5-kilobase transcript (data not shown). This band was absent in both brain and spinal cord. Analysis of RNA from selected rat tissues by RT-PCR (Fig. 2*B*) suggests that PN3 mRNA expression was limited to DRG, nodose ganglia, and to a lesser extent, sciatic nerve of the peripheral nervous system (35 cycles of PCR). No signal was present in the sciatic nerve after 25 cycles of amplification. PN3 mRNA was not detected in brain, spinal cord, superior cervical ganglia, heart, or skeletal muscle after 35 cycles of amplification. Additional RT-PCR analyses of DRG mRNA

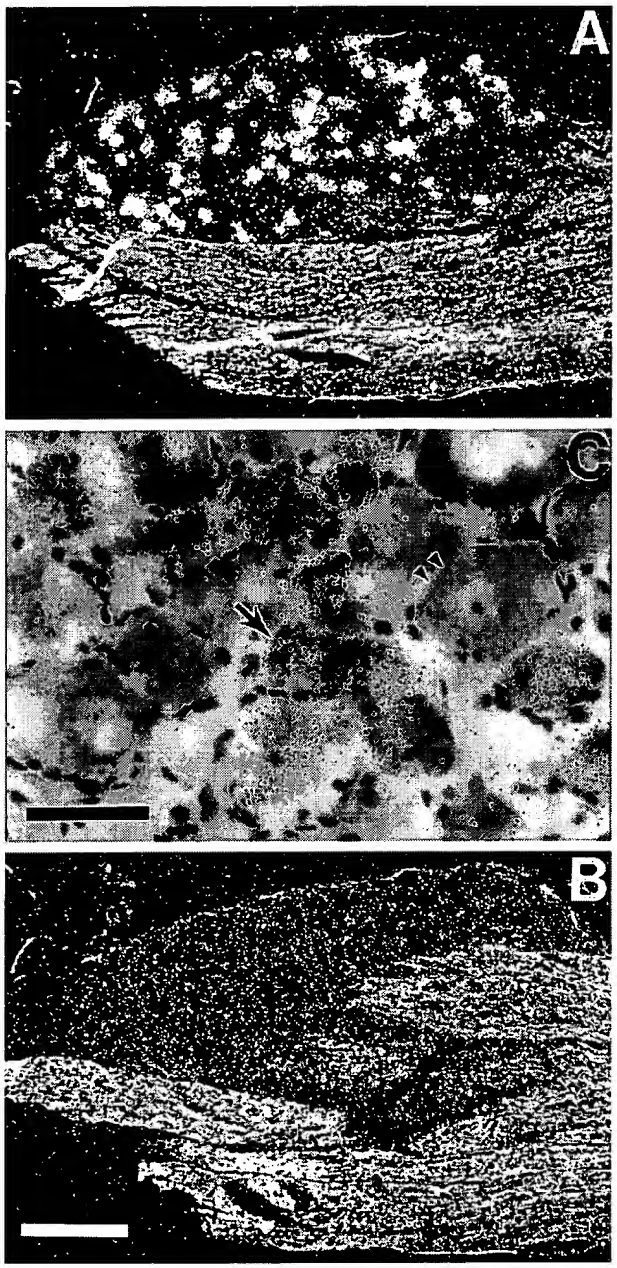

FIG. 3. **Emulsion autoradiography illustrating the distribution of PN3 mRNA in rat DRG.** Dark field photomicrographs of sections hybridized with antisense (*A*) and sense (*B*) strand PN3-specific radiolabeled oligomers. *C*, bright field enlargement of a section hybridized with a radiolabeled antisense probe mixture and counterstained with hematoxylin. Labeled neurons (*arrow*) and unlabeled neurons (*double arrowhead*) were distributed throughout the DRG. Scale: *A* and *B*, 250 μm; *C*, 50 μm.

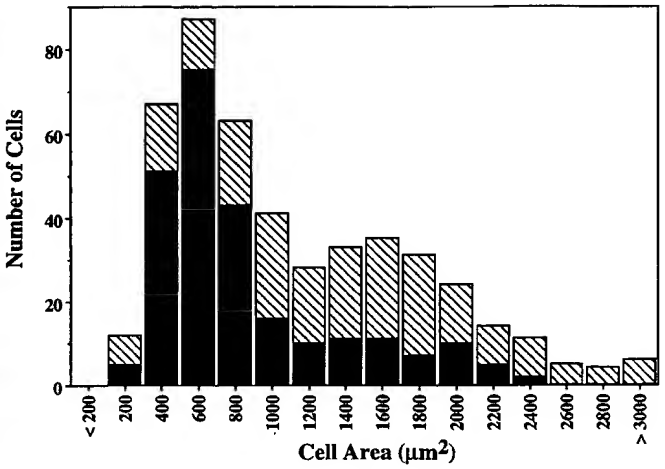

FIG. 4. **Frequency distribution histogram of somal areas from sections through lumbar DRG.** The number of neurons hybridized with PN3 is shown by *filled bars* (n = 246). The number of non-hybridized neurons is shown by *hatched bars* (n = 215).

have detected other sodium channels including rBI (23), rBIII (24), rH1 (25), peripheral nerve sodium channel type 1 (PN1) (26), SCP6 (27), and other novel sodium channel α-subunits (data not shown).

In situ hybridization using PN3-specific oligonucleotide probes showed that PN3 mRNA was expressed predominantly by small neurons in rat DRG (Fig. 3). Approximately 76% of the small cell population (400–1000 μm^2) and 33% of the large cell population (1400–2000 μm^2) were hybridized with probes for PN3 (Fig. 4). Recently, Akopian and Wood (28) isolated a partial cDNA clone, G7, from a rat DRG cDNA library with homology to known sodium channels and specific expression in subsets of sensory neurons. Whether *PN3* and *G7* are the same gene is unknown at present.

Functional Analysis of PN3—Two electrode voltage clamp recordings from *Xenopus* oocytes injected with PN3 cRNA indicated that expression of PN3 produced an inward current with slow inactivation kinetics (Fig. 5*A*). This current was voltage-dependent (Fig. 5*B*) and is carried by sodium ions; reduction of extracellular sodium ion concentration (by substituting *N*-methyl-D-glucamine) from 91 to 50 and 21 mM resulted in hyperpolarizing shifts in the reversal potential from +43 mV to +12 mV and −22 mV, respectively. Examination of the current-voltage relationship for PN3 (Fig. 5*B*) reveals a strikingly depolarized activation potential. In this expression system, PN3 exhibits little or no activation at −10 mV, whereas most cloned sodium channels begin to activate between −60 and −30 mV (29–31).

The currents produced by injection of PN3 cRNA had slow inactivation kinetics (Fig. 5*A*). rBIIa, rBIII, and rSkM1 sodium channels also produce currents with slow inactivation kinetics when injected into *Xenopus* oocytes; coexpression of the β1-subunit greatly accelerates the inactivation kinetics of these channels (22, 32–35). However, coinjection of 1.3 ng of human sodium channel β1-subunit (hSCNβ1) (36) cRNA, which is homologous to the rat brain and DRG SCNβ1, with PN3 cRNA did not accelerate the inactivation kinetics (data not shown). In contrast, coexpression of this quantity of hSCNβ1 cRNA with rSkM1 cRNA was sufficient to accelerate the inactivation kinetics of rSkM1 maximally. Therefore, PN3 may possess inherently slow kinetics.

When expressed in *Xenopus* oocytes, the PN3 sodium current is highly resistant to TTX ($IC_{50} \geq 100$ μM) (Fig. 5*C*). The TTX-sensitive brain and skeletal muscle sodium channels are blocked by nanomolar TTX concentrations, whereas the TTX-insensitive cardiac sodium channels are blocked by micromolar TTX concentrations (2). In rat heart sodium channel 1 (rH1), Cys^{374} is a critical determinant of TTX insensitivity (37–39); in the TTX-sensitive rBI, rBII, rBIII, and rSkM1, the corresponding residue is an aromatic amino acid, either Phe or Tyr, the aromatic ring of which facilitates the binding of TTX to the protein. In PN3, this position is occupied by a Ser residue (Ser^{356}), which may explain the unique response to TTX. Site-directed mutagenesis of this residue to Phe/Tyr or Cys will determine whether this amino acid residue is solely responsible for TTX resistance.

TTX-resistant sodium currents have been implicated in peripheral and central neuronal sensitization mediated by the

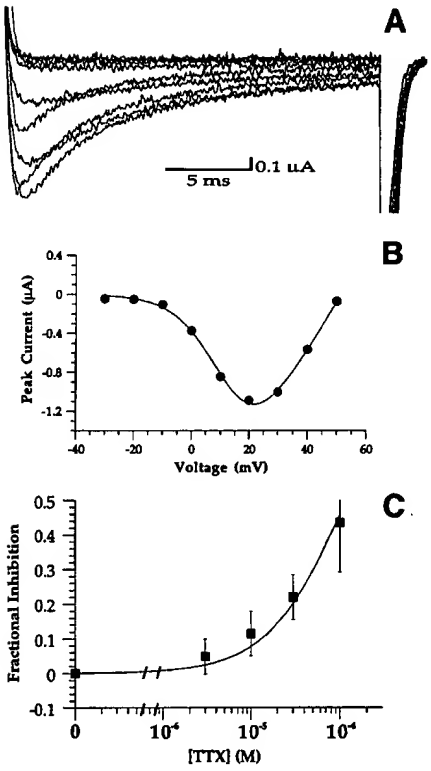

FIG. 5. **Expression of PN3 in *Xenopus* oocytes.** *A*, currents produced by step depolarizations of an oocyte injected with 18 ng of PN3 cRNA from a holding potential of −100 to −30 mV through +50 mV in 10-mV increments. The Geneclamp hardware leak subtraction was used. No inward current was observed in oocytes injected with water. *B*, current-voltage relationship of the data in *A*. *C*, concentration dependence for TTX block of PN3 sodium current. Each oocyte was exposed to the full range of TTX concentrations shown, beginning with the lowest concentration and proceeding to the highest. For each concentration, the effect was allowed to attain steady state. Each *point* represents the mean ± range; $n = 2$.

C-fibers of small neurons following peripheral tissue damage and nerve injury. The biophysical and pharmacological properties of PN3 suggest that it contributes to the TTX-resistant sodium currents in small neurons of DRG. PN3 may, therefore, play a role in the the sensory function and dysfunction that is characteristic of pathophysiological pain processing. In addition, we suggest that PN3 may conduct TTX-resistant sodium currents in other sensory ganglia of the peripheral nervous system such as nodose ganglia (40).

Acknowledgments—We thank C. Yee, P. Zuppan, and C. Bach for sequence analysis and oligonucleotide synthesis. L. Hedley and G. Faurot assisted in DRG isolations. A. L. Goldin and G. Mandel kindly provided plasmid pBSTA and SkM1 plasmid DNA, respectively. We also thank H. Chan, D. Clarke, and R. Whiting for their interest and encouragement during the course of this work.

REFERENCES

1. Catterall, W. A. (1992) *Physiol. Rev.* **72,** S15–S48
2. White, J. A., Alonso, A., and Kay, A. R. (1993) *Neuron* **11,** 1037–1047
3. Kostyuk, P. G., Veselovsky, N. S., and Tsyndrenko, A. Y. (1981) *Neuroscience* **6,** 2423–2430
4. McLean, M. J., Bennett, P. B., and Thomas, R. M. (1988) *Mol. Cell. Biochem.* **80,** 95–107
5. Roy, M. L., and Narahashi, T. (1992) *J. Neurosci.* **12,** 2104–2111
6. Caffrey, J. M., Eng, D. L., Black, J. A., Waxman, S. G., and Kocsis, J. D. (1992) *Brain Res.* **592,** 283–297
7. Elliott, A. A., and Elliott, J. R. (1993) *J. Physiol. (Lond.)* **463,** 39–56
8. Ogata, N., and Tatebayashi, H. (1993) *J. Physiol. (Lond.)* **466,** 9–37
9. Coderre, T. J., Katz, J., Vaccarino, A. L., and Melzack, R. (1993) *Pain* **52,** 259–285
10. Woolf, C. J., and Doubell, T. P. (1994) *Curr. Opin. Neurobiol.* **4,** 525–534
11. Kieffer, B. L. (1991) *Gene (Amst.)* **109,** 115–119
12. Auld, V. J., Goldin, A. L., Krafte, D. S., Marshall, J., Dunn, J. M., Catterall, W. A., Lester, H. A., Davidson, N., and Dunn, R. J. (1988) *Neuron* **1,** 449–461
13. Tso, J. Y., Sun, X.-H. Kao, T.-H., Reece, K. S., and Wu, R. (1985) *Nucleic Acids Res.* **13,** 2485–2502
14. Goldin, A. L. (1992) *Methods Enzymol.* **207,** 266–279
15. Schreibmayer, W., Lester, H. A., and Dascal, N. (1994) *Pflügers Arch.* **426,** 453–458
16. Bezanilla, F., and Armstrong, C. M. (1977) *J. Gen. Physiol.* **70,** 549–566
17. Li, M., West, J. W., Numann, R., Murphy, B. J., Scheuer, T., and Catterall, W. A. (1993) *Science* **261,** 1439–1442
18. Murphy, B. J., Rossie, S., De Jongh, K. S., and Catterall, W. A. (1993) *J. Biol. Chem.* **268,** 27355–27362
19. Gautron, S., Dos Santos, G., Pinto-Henrique, D., Koulakoff, A., Gros, F., and Berwald-Netter, Y. (1992) *Proc. Natl. Acad. Sci. U. S. A.* **89,** 7272–7276
20. George, A. L., Jr., Knittle, T. J., and Tamkun, M. M. (1992) *Proc. Natl. Acad. Sci. U. S. A.* **89,** 4893–4897
21. Felipe, A., Knittle, T. J., Doyle, K. L., and Tamkun, M. M. (1994) *J. Biol. Chem.* **269,** 30125–30131
22. Isom, L. L., De Jongh, K. S., Patton, D. E., Reber, B. F., Offord, J., Charbonneau, H., Walsh, K., Goldin, A. L., and Catterall, W. A. (1992) *Science* **256,** 839–842
23. Noda, M., Ikeda, T., Kayano, T., Suzuki, H., Takeshima, H., Kurasaki, M., Takahashi, H., and Numa, S. (1986) *Nature* **320,** 188–192
24. Kayano, T., Noda, M., Flockerzi, V., Takahashi, H., and Numa, S. (1988) *FEBS Lett.* **228,** 187–194
25. Rogart, R. B., Cribbs, L. L., Muglia, L. K., Kephart, D., and Kaiser, M. W. (1989) *Proc. Natl. Acad. Sci. U. S. A.* **86,** 8170–8174
26. D'Arcangelo, G., Paradiso, K., Shepard, D., Brehm, P., Halegoua, S., and Mandel, G. (1993) *J. Cell Biol.* **122,** 915–921
27. Schaller, K. L., Krzemien, D. M., Yarowsky, P. J., Krueger, B. K., and Caldwell, J. H. (1995) *J. Neurosci.* **15,** 3231–3242
28. Akopian, A. N., and Wood, J. N. (1995) *J. Biol. Chem.* **270,** 21264–21270
29. Cribbs, L., Satin, J., Fozzard, H. A., and Rogart, R. B. (1990) *FEBS Lett.* **275,** 195–200
30. Patton, D. E., and Goldin, A. L. (1991) *Neuron* **7,** 637–647
31. Trimmer, J. S., Cooperman, S. S., Tomiko, S. A., Zhou, J. Y., Crean, S. M., Boyle, M. B., Kallen, R. G., Sheng, Z. H., Barchi, R. L., Sigworth, F. J., Goodman, R. H., Agnew, W. S., and Mandel, G. (1989) *Neuron* **3,** 33–49
32. Cannon, S. C., McClatchey, A. I., and Gusella, J. F. (1993) *Pflügers Arch.* **423,** 155–157
33. Wallner, M., Weigel, L., Meera, P., and Lotan, I. (1993) *FEBS Lett.* **336,** 535–539
34. Yang, J. S., Bennet, P. B., Makita, N., George, A. L., and Barchi, R. L. (1993) *Neuron* **11,** 915–922
35. Patton, D. E., Isom, L. L., Catterall, W. A., and Goldin, A. L. (1994) *J. Biol. Chem.* **269,** 17649–17655
36. McClatchey, A. L., Cannon, S. C., Slaugenhaupt, S. A., and Gusella, J. F. (1993) *Hum. Mol. Genet.* **2,** 745–749
37. Backx, P. H., Yue, D. T., Lawrence, J. H., Marban, E., and Tomaselli, G. F. (1992) *Science* **257,** 248–251
38. Chen, L.-Q., Chahine, M., Kallen, R. G., Barch, R. L., and Horn, R. (1992) *FEBS Lett.* **309,** 253–257
39. Satin, J., Kyle, J. W., Chen, M., Bell, P., Cribbs, L. L., Fozzard, H. A., and Rogart, R. B. (1992) *Science* **256,** 1202–1205
40. Ikeda, S. R., Schofield, G. G., and Weight, F. F. (1986) *J. Neurophysiol.* **55,** 527–539

KCNQ2 and KCNQ3 Potassium Channel Subunits: Molecular Correlates of the M-Channel

Hong-Sheng Wang, Zongming Pan, Wenmei Shi, Barry S. Brown, Randy S. Wymore, Ira S. Cohen, Jane E. Dixon,* David McKinnon

The M-current regulates the subthreshold electrical excitability of many neurons, determining their firing properties and responsiveness to synaptic input. To date, however, the genes that encode subunits of this important channel have not been identified. The biophysical properties, sensitivity to pharmacological blockade, and expression pattern of the KCNQ2 and KCNQ3 potassium channels were determined. It is concluded that both these subunits contribute to the native M-current.

The M-current is a slowly activating and deactivating potassium conductance that plays a critical role in determining the subthreshold electrical excitability of neurons as well as the responsiveness to synaptic inputs (*1–3*). The M-current was first described in peripheral sympathetic neurons (*4*, *5*), and differential expression of this conductance produces subtypes of sympathetic neurons with distinct firing patterns (*3*). The M-current is also expressed in many neurons in the central nervous system (CNS) (*1*, *6*, *7*).

To date, the molecular identity of the channels underlying the M-current remains unknown. Here we show that the KCNQ2 and KCNQ3 channel subunits can coassemble to form a channel with essentially identical biophysical properties and pharmacological sensitivities to the native M-current and that the pattern of *KCNQ2* and *KCNQ3* gene expression is consistent with these genes encoding the native M-current.

The KCNQ potassium channel gene family has three members: KCNQ1 (KvLQT1), KCNQ2, and KCNQ3 (*8–12*). Injection of KCNQ2 mRNA into *Xenopus* oocytes resulted in the consistent expression of a relatively small potassium current that is slowly activating and deactivating (Fig. 1A). The properties of this channel are essentially identical to those described previously (*11*). In contrast, injection of KCNQ3 mRNA did not result in the expression of a current above background level. When the KCNQ2 and KCNQ3 mRNAs were coinjected, however, the resultant current was 11-fold larger than that found in cells injected with KCNQ2 mRNA alone (Fig. 1, A and B). The large increase in current density after coinjection of KCNQ3 mRNA suggests that the KCNQ3 subunit facilitates expression of the KCNQ2 subunits, possibly by the formation of a heteromeric complex of KCNQ2 and KCNQ3 subunits. Expression of a relatively small current after KCNQ3 mRNA injection into oocytes has been reported (*13*), suggesting that the KCNQ3 subunit can function as a homomeric channel under some experimental conditions. It is possible, however, that assembly with the endogenous *Xenopus* KCNQ subunit (*14*) may facilitate KCNQ3 expression in these experiments.

In addition to affecting current density, the KCNQ3 subunit affects the sensitivity of the KCNQ2 channel to blockade by tetraethylammonium (TEA). The homomultimeric KCNQ2 channel was very sensitive to TEA [dissociation constant (K_d) = 0.16 ± 0.02 mM, n = 5], whereas channels expressed after coinjection of KCNQ2 and KCNQ3 mRNAs were much less sensitive (K_d = 3.5 ± 0.7 mM, n = 6). The KCNQ2 and KCNQ3 subunits differ within the pore region, at a position that determines sensitivity to blockade by TEA (Fig. 1C). The KCNQ2 subunit has a tyrosine residue at this position, which confers high sensitivity to TEA, whereas the KCNQ3 channel has a threonine residue, which confers low sensitivity to TEA (*15*). The intermediate sensitivity to TEA block of the KCNQ2+KCNQ3 channels confirms that the KCNQ2 and KCNQ3 subunits coassemble into a heteromultimeric complex (Fig. 1D), in a manner closely analogous to heteromultimers of *Shaker* channels (*16*). For comparison, the native M-current in rat sympathetic neurons is also moderately sensitive to blockade by TEA [median inhibitory concentration (IC_{50}) = 5.8 ± 0.2 mM, n = 3], as is the M-current found in hippocampal and olfactory cortex neurons (*6*). It seems likely, therefore, that if the KCNQ2 and KCNQ3 subunits contribute to the native M-channel, they assemble as a heteromultimeric complex with expression of both subunits required to achieve normal current levels and pharmacological properties.

The kinetic properties of the KCNQ2+KCNQ3 channel were markedly similar to

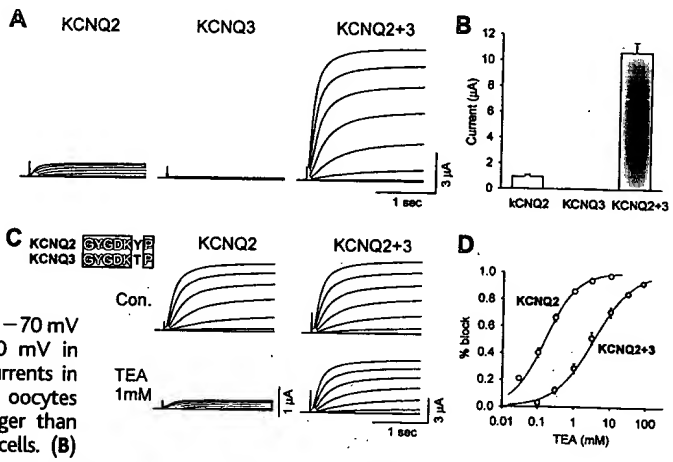

Fig. 1. The KCNQ2 and KCNQ3 potassium channel subunits form heteromultimers. **(A)** Currents recorded in *Xenopus* oocytes after injection of KCNQ2 mRNA, KCNQ3 mRNA, or an equimolar ratio of KCNQ2 and KCNQ3 mRNAs (*30*, *31*). Currents elicited by 2-s voltage steps from a holding potential of −70 mV over the range −60 to 0 mV in 10-mV increments. The currents in KCNQ3 mRNA–injected oocytes were not substantially larger than those seen in uninjected cells. **(B)** Histogram showing the average current response to a voltage-clamp step to 0 mV from −70 mV in cells injected with KCNQ2, KCNQ3, or an equimolar ratio of KCNQ2 and KCNQ3 mRNAs (45 ng of each mRNA was injected per oocyte). Average current responses in the three sets of cells were significantly different to each other ($P < 0.001$, n = 19 to 22). **(C)** Effect of 1 mM TEA on currents elicited from oocytes injected with KCNQ2 mRNA or an equimolar ratio of KCNQ2 and KCNQ3 mRNAs. The voltage clamp protocol was the same as that used in (A). The KCNQ2+KCNQ3 mRNA mixture was diluted to reduce current density. **(Inset)** Comparison of the deduced amino acid sequence in the pore region around the residue controlling TEA sensitivity [equivalent to position 449 in the *Shaker* H4 channel (*16*)]. D, Asp; G, Gly; K, Lys; P, Pro; T, Thr; Y, Tyr. **(D)** Dose-response curves for TEA block of KCNQ2 channels and KCNQ2+KCNQ3 channels. Figure shows averaged data fitted with the Hill equation with average parameters obtained from fits to individual cells. For KCNQ2, K_d = 0.16 ± 0.02 mM (n = 5) and the Hill coefficient was set to unity. For KCNQ2+KCNQ3, K_d = 3.5 ± 0.7 mM, Hill coefficient = 0.82 ± 0.03 (n = 6).

H.-S. Wang, R. S. Wymore, I. S. Cohen, J. E. Dixon, Institute of Molecular Cardiology, Department of Physiology and Biophysics, State University of New York at Stony Brook, Stony Brook, NY 11794, USA. Z. Pan, W. Shi, D. McKinnon, Department of Neurobiology and Behavior, State University of New York at Stony Brook, Stony Brook, NY 11794, USA. B. S. Brown, CNS Diseases Research, DuPont Pharmaceuticals, Wilmington, DE 19880, USA.

*To whom correspondence should be addressed.

those of the native M-current. Characteristic kinetic properties of the M-current include a relatively negative activation curve, a substantial steady-state conductance at −30 mV, and slow activation and deactivation kinetics (*3*, *5*). By use of the classic M-current voltage-clamp protocol (*4*), the KCNQ2+KCNQ3 channel closely replicated the waveform of the native M-current (Fig. 2A). The activation waveform was similar for the two currents, although the native current appeared to activate slightly faster (Fig. 2B). The conductance-voltage curves were very similar for the two channel types with the threshold for activation near −60 mV and most of the channels activated at −30 mV (Fig. 2C). The deactivation kinetics of the M-current are biphasic (*17*), and this was also true for the KCNQ2+KCNQ3 channel (Fig. 2D). Both channel types had similar time constants for the two components of deactivation. Deactivation time constants at −50 mV for the M-current were 145 ± 25 ms and 838 ± 125 ms (fast component, 55 ± 3% of total; n = 4), and for KCNQ2+KCNQ3 were 171 ± 12 ms and 857 ± 146 ms (fast component, 49 ± 3%; n = 9). At −60 mV these values were, for the M-current, 126 ± 28 ms and 934 ± 117 ms (fast component, 60 ± 2%; n = 4), and for KCNQ2+KCNQ3, 149 ± 9 ms and 741 ± 69 ms (fast component, 59 ± 3%; n = 9). For both the native M-current and the KCNQ2+KCNQ3 channels, the time constant of the fast component was voltage sensitive (Fig. 2E), whereas the slow component was relatively insensitive to voltage over the same voltage range.

Although the kinetic properties of the KCNQ2+KCNQ3 channel were very similar to those of the native M-current, it is important to establish other criteria that can be used to determine the molecular identity of the native conductance. One obvious approach is to determine the sensitivity of candidate channels to muscarinic inhibition, the characteristic that gives the M-current its name. We find that the KCNQ2+KCNQ3 channel is strongly inhibited by muscarine when coexpressed in *Xenopus* oocytes with the m_1 muscarinic receptor (*18*). This criterion is too broad to be very useful for at least two reasons. First, a wide range of potassium currents in addition to the M-current are inhibited in sympathetic neurons after muscarinic receptor stimulation (*19*). Second, many different cloned potassium channels are inhibited after stimulation of coexpressed m_1 muscarinic receptors. The M-current is sensitive to blockade by Ba^{2+} ions (*1*) and the KCNQ2+KCNQ3 channel is similarly sensitive (67 ± 3% block by 1 mM Ba^{2+}, n = 5). This criterion is also too broad, however, with many other potassium channels showing a similar sensitivity to Ba^{2+} ions.

Another approach is the use of selective blocking drugs. Two drugs that are useful in establishing the identity of the M-channel are linopirdine and 10,10-*bis*(4-pyridinylmethyl)-9(10 H)-anthracenone (XE991) (*20*). Linopirdine blocks the M-current at micromolar concentrations by direct channel blockade (*21*–*23*). The IC_{50} for block of the M-channel in sympathetic neurons by linopirdine is in the range 3.4 to 7.0 μM (*22*, *23*).

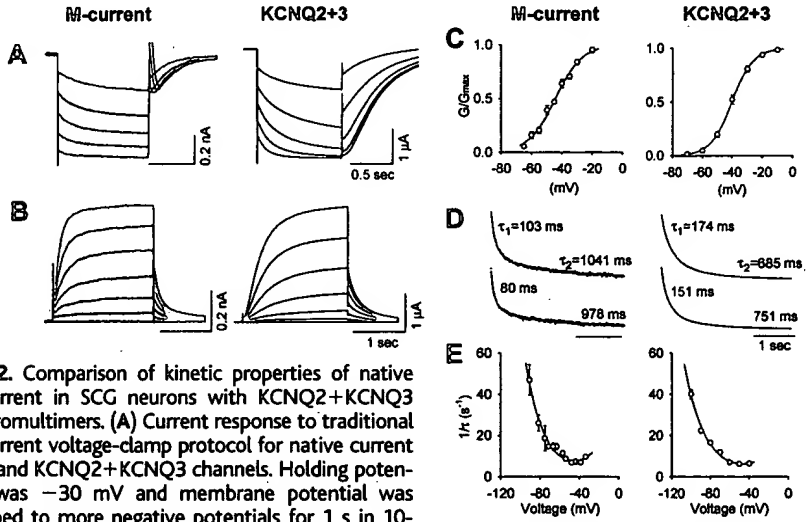

Fig. 2. Comparison of kinetic properties of native M-current in SCG neurons with KCNQ2+KCNQ3 heteromultimers. (**A**) Current response to traditional M-current voltage-clamp protocol for native current (*32*) and KCNQ2+KCNQ3 channels. Holding potential was −30 mV and membrane potential was stepped to more negative potentials for 1 s in 10-mV increments. Apparent differences in the current waveforms are largely due to the presence of a linear leak current in the recordings from SCG neurons that is relatively smaller in the oocytes. The initial phase of M-current reactivation in SCG neurons is obscured by activation of the A-current. (**B**) Activation of M-current and KCNQ2+KCNQ3 channels from a holding potential of −60 mV in 5-mV increments. (**C**) Conductance-voltage curves fitted with a single Boltzmann function. For the native M-current the fit is to averaged data points, with V_n = −44 mV and k_n = −8.8 mV (n = 6, bars are SEMs). For KCNQ2+KCNQ3 channels, V_n = −40 ± 1 mV and k_n = −6.8 ± 0.1 mV (n = 6, bars are SEMs). Conductance-voltage curves for KCNQ2+KCNQ3 channels were constructed with tail currents at −60 mV after depolarizing voltage steps from a holding potential of −70 mV. (**D**) Deactivation process had two time constants for both channel types. Time constants for deactivation are shown next to current traces for steps from −30 mV holding potential to −50 mV (top trace) or −60 mV. Biexponential fits are superimposed on the experimental data. (**E**) Reciprocal time constant for fast deactivation of the native M-current and KCNQ2+KCNQ3 channels. Data points are averages from three to nine cells for the native M-current and nine cells for KCNQ2+KCNQ3. Data were fitted with the equation (*5*) $1/\tau = \alpha_0(\beta_0)\exp[\pm(V_m - V_0)/y]$, where V_m is the membrane potential, $\alpha_0(\beta_0)$ = 3.8 s^{-1}, V_0 = −45.4 mV, and y = 18.3 mV for the native M-current and $\alpha_0(\beta_0)$ = 3.0 s^{-1}, V_0 = −46.7 mV, and y = 20.9 mV for the KCNQ2+KCNQ3 channel. The native M-current was recorded from SCG neurons in intact, isolated ganglia and the KCNQ2+KCNQ3 currents were recorded in *Xenopus* oocytes, both at room temperature.

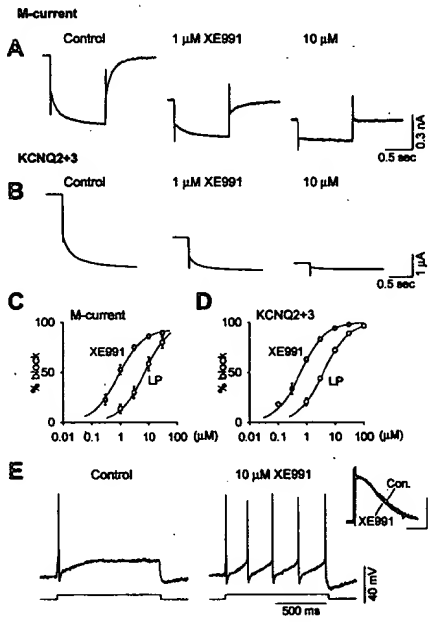

Fig. 3. Channel blockade by XE991 of the M-current and KCNQ2+KCNQ3 channels. (**A**) Blockade of M-current in SCG neurons by XE991. Holding potential was −30 mV and step potential was −50 mV for 1 s. The shift in holding current after drug application is due to the inhibition of M-current activated at the holding potential. (**B**) Blockade of KCNQ2+KCNQ3 channels by XE991. Holding potential was −60 mV and the cell was repetitively depolarized to −30 mV for 1 min to reach steady-state blockade. Tail currents were recorded at −60 mV. (**C** and **D**) Dose-response curves for linopirdine (○) and XE991 (○) for blockade of M-current (C) and KCNQ2+KCNQ3 channels (D). Maximal block was 93 ± 2% of native M-current and 100% of KCNQ2+KCNQ3 channels. Data points are averages and error bars represent SEMs. (**E**) Effect of 10 μM XE991 on the firing properties of a phasic sympathetic neuron recorded from the SCG. Membrane potential was held at −60 mV and the depolarizing current step was 0.2 nA for control and XE991 application. (**Inset**) Voltage-clamp recording of the I_{AHP} before and after application of 10 μM XE991. Recordings were done as described (*3*). Calibration bar, 200 ms and 0.1 nA.

The related compound XE991 has an IC_{50} of 0.98 ± 0.15 μM (Fig. 3C). Only one class of voltage-gated potassium channels had a pharmacological profile similar to that of the native M-current: the KCNQ channels, which were blocked by both XE991 and linopirdine at very similar concentrations to the native M-current (Table 1). Of particular interest was XE991, which had both high affinity and selectivity for the native M-channel and KCNQ channels. No *eag*- or *Shaker*-related channel tested had a similar sensitivity. Unlike the KCNQ2 and KCNQ3 channels, the KCNQ1 channel cannot contribute to the native M-channel because the *KCNQ1* gene is not expressed in either sympathetic ganglia (*24*) or the CNS (*8*).

Consistent with the high selectivity of XE991 for the M-current is its effect on the firing properties of sympathetic neurons. In the rat, there are two classes of sympathetic neurons: phasic-firing neurons, which have a relatively large M-current, and tonic-firing neurons, which do not express an M-current (*3*). We have shown previously that differential expression of the M-current is the primary determinant of the different firing properties of phasic and tonic neurons (*3*). This conclusion is confirmed by the observation that blocking the M-current in phasic neurons with 10 μM XE991 converts the firing properties from phasic to tonic without affecting any other electrophysiological properties, including the slow after-hyperpolarization (Fig. 3E).

The expression pattern of *KCNQ2* and *KCNQ3* genes in sympathetic ganglia is consistent with these genes encoding subunits of the M-channel. The expression of multisubunit proteins is often regulated by limiting the expression of a single subunit, and this is apparently true for the M-current. The superior cervical ganglia (SCG) contain only phasic neurons, whereas the prevertebral sympathetic ganglia (celiac ganglia and superior mesenteric ganglia) contain predominantly tonic neurons (Fig. 4A). The gene regulating expression of the M-channel should, therefore, be expressed at substantially lower levels in prevertebral sympathetic ganglia than in the SCG, and *KCNQ2* gene expression does in fact closely parallel M-current expression in these ganglia (Fig. 4B). Of the 24 different voltage-gated potassium channel genes tested to date, no other gene has a similar expression pattern in sympathetic ganglia (*25*, *26*). The *KCNQ3* gene was expressed at approximately equal levels in both SCG and prevertebral ganglia (Fig. 4C). The KCNQ3 subunit expresses poorly or not at all when expressed by itself in vitro and it is likely, therefore, that M-current expression in sympathetic ganglia is determined primarily by regulation of *KCNQ2* gene expression.

In the CNS, the M-current is expressed in many neurons in the cortex and hippocampus but has not been described in the cerebellum. In contrast to the peripheral nervous system, *KCNQ2* gene expression does not parallel M-current expression in these CNS regions, and the *KCNQ2* gene was expressed at relatively high levels in all three regions (Fig. 4D). The *KCNQ3* gene, however, was expressed at much lower levels in the cerebellum than in cortex and hippocampus, like the M-current (Fig. 4E), suggesting that regulation of *KCNQ3* gene expression is also important in determining M-current expression levels in vivo. This conclusion is consistent with the in vitro results demonstrating that expression of the KCNQ2+KCNQ3 heteromultimeric channel is much more efficient than that of the KCNQ2 homomultimer.

Taken together, these results strongly suggest that the KCNQ2 and KCNQ3 subunits contribute to the native M-channel. The KCNQ2+KCNQ3 channel is the only known potassium channel that can reproduce the unique kinetic properties of the native M-cur-

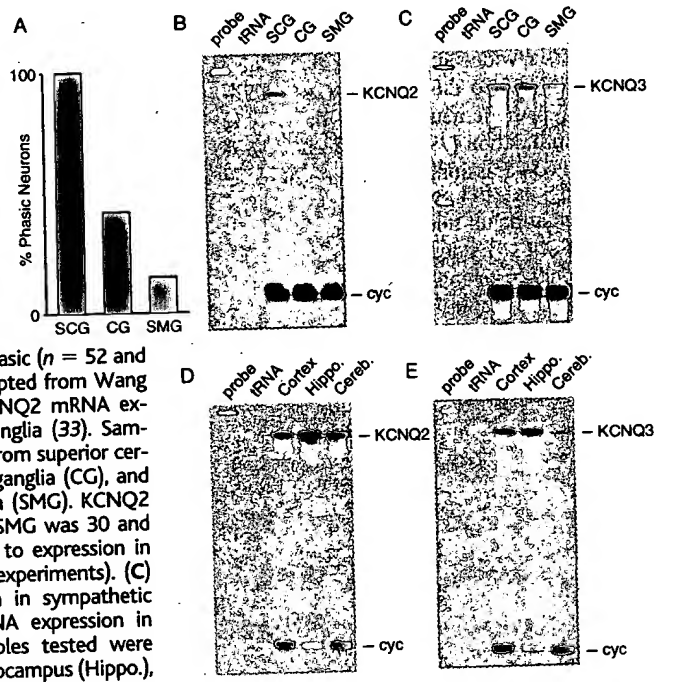

Fig. 4. KCNQ2 and KCNQ3 mRNA expression in different rat sympathetic ganglia and brain regions determined by RNase protection analysis. **(A)** Histogram showing the distribution of phasic neurons in prevertebral and paravertebral sympathetic ganglia. Neurons in SCG are exclusively phasic (n = 36), whereas only 42% of the neurons in the CG and 15% in SMG are phasic (n = 52 and 40, respectively). [Data adapted from Wang and McKinnon (*3*).] **(B)** KCNQ2 mRNA expression in sympathetic ganglia (*33*). Samples tested were prepared from superior cervical ganglia (SCG), celiac ganglia (CG), and superior mesenteric ganglia (SMG). KCNQ2 expression in the CG and SMG was 30 and 19%, respectively, relative to expression in the SCG (average of two experiments). **(C)** KCNQ3 mRNA expression in sympathetic ganglia. **(D)** KCNQ2 mRNA expression in three brain regions. Samples tested were prepared from cortex, hippocampus (Hippo.), and cerebellum (Cereb.). **(E)** KCNQ3 mRNA expression in three brain regions. All samples contained 5 μg of total RNA, and the cyclophilin gene (cyc) was used as a positive internal control and yeast tRNA as a negative control.

Table 1. Comparison of M-current and cloned potassium channels: IC_{50} for linopirdine and XE991 blockade. The number of cells is indicated in parentheses. IC_{50} values (mean ± SEM) are expressed in micromolar. In cases where the IC_{50} values were >100 μM, the exact value is not reported owing to limited solubility of the drug. It has been suggested that *eag*-related potassium channels might encode the M-current (*29*), and all the *eag*-related channels expressed in SCG (*26*) were tested in addition to representative examples of delayed-rectifier and A-channels.

M-current	KCNQ2 +KCNQ3	KCNQ2	KCNQ1	eag1	erg1	erg3	elk1	Kv1.2	Kv4.3
XE991									
0.98 ± 0.15 (3)	0.6 ± 0.1 (6)	0.71 ± 0.07 (6)	0.75 ± 0.05 (7)	49 ± 6* (6)	>100 (4)	>100 (6)	>100 (5)	>100 (5)	43 ± 7 (5)
Linopirdine									
7.0 ± 1.1† (5)	4.0 ± 0.5 (6)	4.8 ± 0.6 (5)	8.9 ± 0.9 (6)	31 ± 3* (9)	53 ± 4 (6)	85 ± 5 (5)	37 ± 4‡ (7)	68 ± 6 (4)	86 ± 14 (4)

*Blockade of the eag1 channel was incomplete with 82 ± 1% (n = 4) blockade by 1 mM linopirdine and 56 ± 2% (n = 6) blockade by 100 μM XE991. †Data adapted from Costa and Brown (*23*); a similar value of 3.4 ± 0.3 μM was obtained by Lamas *et al.* (*22*). ‡The IC_{50} for block of elk1 channels by linopirdine was highly voltage dependent, and the value shown is for a step to −10 mV: IC_{50} values ranged from 26 ± 3 μM at −20 mV (n = 7) to 144 ± 10 μM at +30 mV (n = 3).

rent, and several different pharmacological agents have very similar effects on the native M-current and the KCNQ2+KCNQ3 channel. In particular, the compound XE991 is highly selective for both the M-current and KCNQ channels. Finally, the *KCNQ2* gene is the only known potassium channel gene that is expressed in a pattern that parallels the distribution of the M-current in peripheral sympathetic ganglia. These data make a compelling case for the hypothesis that the KCNQ2+KCNQ3 channel is a molecular correlate of the M-current in sympathetic neurons.

The *KCNQ2* and *KCNQ3* genes are also abundantly expressed in the CNS, and it is likely that the KCNQ2+KCNQ3 subunits contribute to the M-current in central neurons. This conclusion is consistent with the observation that mutations in either the *KCNQ2* or *KCNQ3* genes result in an inherited autosomal dominant epilepsy (*10–12*). The very similar phenotypes produced by mutations in either of these two distinct genes (*27*) can be explained by the observation that both gene products are required to produce full expression of functional channels. Identification of the physiological function of the channel encoded by the *KCNQ2* and *KCNQ3* genes may facilitate the development of symptomatic treatments for these epilepsies.

References and Notes

1. D. A. Brown, in *Ion Channels*. T. Narahashi, Ed. (Plenum, New York, 1988), pp. 55–94.
2. W. M. Yamada, C. Koch, P. R. Adams, in *Methods in Neuronal Modeling*, C. Koch and I. Segev, Eds. (Bradford, Cambridge, MA, 1989), pp. 97–133.
3. H.-S. Wang and D. McKinnon, *J. Physiol.* **485**, 319 (1995).
4. D. A. Brown and P. R. Adams, *Nature* **283**, 673 (1980).
5. A. Constanti and D. A. Brown, *Neurosci. Lett.* **24**, 289 (1981).
6. J. F. Storm, *J. Physiol.* **409**, 171 (1989); A. Constanti and J. A. Sim, *ibid.* **387**, 173 (1987).
7. M. D. Womble and H. C. Moises, *ibid.* **457**, 93 (1992).
8. Q. Wang *et al.*, *Nature Genet.* **12**, 17 (1996).
9. A. Wei, T. Jegla, L. Salkoff, *Neuropharmacology* **35**, 805 (1996).
10. N. A. Singh *et al.*, *Nature Genet.* **18**, 25 (1998).
11. C. Biervert *et al.*, *Science* **279**, 403 (1998).
12. C. Charlier *et al.*, *Nature Genet.* **18**, 53 (1998).
13. Yang *et al.*, *J. Biol. Sci.* **273**, 19419 (1998).
14. M. C. Sanguinetti *et al.*, *Nature* **384**, 80 (1996).
15. R. MacKinnon and G. Yellen, *Science* **250**, 276 (1990).
16. L. Heginbotham and R. MacKinnon, *Neuron* **8**, 483 (1992).
17. N. V. Marrion, P. R. Adams, W. Gruner, *Proc. R. Soc. London Ser. B* **248**, 207 (1992).
18. H.-S. Wang *et al.*, data not shown. KCNQ2, KCNQ3, and m_1 muscarinic receptor mRNAs were coinjected, and inhibition after application of 10 μM muscarine was measured.
19. J. F. Cassell and E. M. McLachlan, *Br. J. Pharmacol.* **91**, 259 (1987); H.-S. Wang and D. McKinnon, *J. Physiol.* **492**, 467 (1996).
20. R. Zaczek *et al.*, *J. Pharmacol. Exp. Ther.* **285**, 724 (1998).
21. S. P. Aiken, B. J. Lampe, P. A. Murphy, B. S. Brown, *Br. J. Pharmacol.* **115**, 1163 (1995).
22. J. A. Lamas, A. A. Selyanko, D. A. Brown, *Eur. J. Neurosci.* **9**, 605 (1997).
23. A. M. N. Costa and B. S. Brown, *Neuropharmacology* **36**, 1747 (1997).
24. H.-S. Wang *et al.*, data not shown. Ribonuclease (RNase) protection assay of SCG RNA was done with a rat KCNQ1-specific probe.
25. J. E. Dixon and D. McKinnon, *Eur. J. Neurosci.* **8**, 183 (1996).
26. W. Shi *et al.*, *J. Neurosci.* **17**, 9423 (1997); W. Shi *et al.*, *J. Physiol.* **511**, 675 (1998).
27. O. Steinlein *et al.*, *Hum. Genet.* **95**, 411 (1995).
28. J. E. Dixon *et al.*, *Circ. Res.* **79**, 659 (1996).
29. C. E. Stansfeld *et al.*, *Trends Neurosci.* **20**, 13 (1997).
30. The *KCNQ3* gene was initially identified as an expressed sequence tag in a search of GenBank (accession number AA001392). On the basis of this sequence, primers were designed and used to amplify partial KCNQ3 cDNA clones from rat brain and SCG cDNA by polymerase chain reaction (PCR). We determined an initial sequence encompassing the entire open reading frame of the *KCNQ3* gene by performing several rounds of 5′ and 3′ RACE (rapid amplification of cDNA ends) PCR using initial anchor oligonucleotides complementary to the partial cDNA clone and SCG cDNA as a template for amplification. Once cDNAs were obtained that extended beyond both the 5′ and 3′ ends of the open reading frame, oligonucleotides complementary to noncoding regions at either end of the coding sequence were designed. We amplified multiple full-length cDNA clones in independent PCR reactions from rat SCG cDNA using Expand Long Template PCR (Boehringer Mannheim, Indianapolis, IN) with several combinations of the following oligonucleotides: TTGACTCCCCATCCGACCT and GCCTTTGCCTTCTTTTGGG (forward reaction), and ACCGCGCACATGCATG and GTGACATGGGGAGGAAGAA (reverse reaction). Four independent clones were sequenced in their entirety in both directions by automatic sequencing (GenBank accession number AF091247). The deduced amino acid sequence was 95% identical to a recently described partial human KCNQ3 cDNA clone (*12*).
31. We amplified full-length KCNQ2 cDNAs from adult human brain cDNA using primers CCCCGCTGAGCCTGAG and TGTAAAAGGTCACTGCCAGG with the Expand High Fidelity enzyme mixture (Boehringer Mannheim). The KCNQ2 cDNA clone used in the biophysical studies was identical to the KCNQ2 cDNA isolated previously from a fetal brain cDNA library (*10*) with the exception of a small deletion in the carboxy intracellular domain (30 amino acids from residues 417 to 446). This region is also alternatively spliced in the KCNQ2 cDNA clone described by Biervert *et al.* (*11*). Preparation, injection of complementary RNA, and recording from oocytes were done as described (*28*). The standard extracellular recording solution contained 82 mM NaCl, 2 mM KCl, 1.8 mM $CaCl_2$, 1 mM $MgCl_2$, and 5 mM Na-Hepes (pH 7.6). Data collection and analysis were done with pClamp software (Axon Instruments, Foster City, CA).
32. Recordings of the M-current in sympathetic neurons in intact ganglia were done at room temperature as described (*3*). The standard extracellular recording solution contained NaCl (133 mM), KCl (4.7 mM), NaH_2PO_4 (1.3 mM), $NaHCO_3$ (16.3 mM), $CaCl_2$ (2 mM), $MgCl_2$ (1.2 mM), and glucose (1.4 g/liter) in an atmosphere of 95% O_2–5% CO_2 to give pH 7.2 to 7.4. Linopirdine and XE991 were from DuPont Pharmaceuticals (Wilmington, DE).
33. Preparation of RNA, RNase protection assays, and isolation of a specific rat KCNQ2 and KCNQ3 probes were done as described (*25*). RNA expression was quantitated directly from dried gels with a PhosphorImager (Molecular Dynamics, Sunnyvale, CA).

34. We thank P. Adams for help and support throughout the course of this work, J. Keast for comments on the manuscript, P. McKinnon for technical assistance, and the anonymous reviewers for suggestions. Supported by grants from the National Institutes of Health.

17 June 1998; accepted 27 October 1998

Linkage of ATM to Cell Cycle Regulation by the Chk2 Protein Kinase

Shuhei Matsuoka, Mingxia Huang, Stephen J. Elledge*

In response to DNA damage and replication blocks, cells prevent cell cycle progression through the control of critical cell cycle regulators. We identified Chk2, the mammalian homolog of the *Saccharomyces cerevisiae* Rad53 and *Schizosaccharomyces pombe* Cds1 protein kinases required for the DNA damage and replication checkpoints. Chk2 was rapidly phosphorylated and activated in response to replication blocks and DNA damage; the response to DNA damage occurred in an ataxia telangiectasia mutated (ATM)–dependent manner. In vitro, Chk2 phosphorylated Cdc25C on serine-216, a site known to be involved in negative regulation of Cdc25C. This is the same site phosphorylated by the protein kinase Chk1, which suggests that, in response to DNA damage and DNA replicational stress, Chk1 and Chk2 may phosphorylate Cdc25C to prevent entry into mitosis.

When DNA is damaged, cells activate a response pathway that arrests the cell cycle and induces the transcription of genes that facilitate repair. The failure of this response results in genomic instability, a mutagenic condition that predisposes organisms to cancer. In eukaryotes, this checkpoint pathway initiated by DNA damage consists of several protein kinases, including the phosphoinositide kinase (PIK) homologs ATM, ATR, Mec1, and Rad3 and the protein kinases Rad53, Cds1, Chk1, and Dun1 (*1*). In mammals, in response to DNA damage, ATM controls cell cycle arrest in G_1 and G_2 and also prevents ongoing DNA synthesis (*1*). ATM controls G_1 arrest by activation of p53 (*2*), which induces transcription of the Cdk

Howard Hughes Medical Institute, Verna and Marrs McLean Department of Biochemistry and Department of Molecular and Human Genetics, Baylor College of Medicine, One Baylor Plaza, Houston, TX 77030, USA.

*To whom correspondence should be addressed. E-mail: selledge@bcm.tmc.edu

VOLUME 282 4 DECEMBER 1998 NUMBER 5395

Science

www.sciencemag.org

COVER Male and female American redstarts migrate from tropical wintering quarters to breeding areas in the United States and Canada each spring. Carbon isotope signatures from birds in the tropics provide a way to link events occurring during these two geographically distinct periods of the annual cycle. [Painting: John P. O'Neill, Museum of Natural Science, Louisiana State University]

1800

NSF's $600 million education experiment

NEWS

NEWS OF THE WEEK

NEWS FOCUS

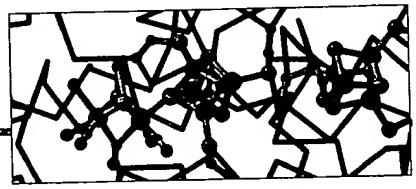

RESEARCH

RESEARCH ARTICLES

REPORTS

DEPARTMENTS

AMERICAN ASSOCIATION FOR THE ADVANCEMENT OF SCIENCE

150 YEARS • 1848-1998

SCIENCE (ISSN 0036-8075) is published weekly on Friday, except the last week in December, by the American Association for t Science, 1200 New York Avenue, NW, Washington, DC 20005. Periodicals Mail postage (publication No. 484460) paid at Washingtor mailing offices. The title SCIENCE is a registered trac Domestic individual membership and subscription (51 issues): $108 ($60 allocated to subscription). Domestic institutional subscriptic Foreign postage extra: Mexico, Caribbean (surface mail) $55; other countries (air assist delivery) $90. First class, airmail, student, ar request. Canadian rates with GST available upon request, GST #1254 88122. IPM #1069624. Printed in the U.S.A.

SCIENCE'S COMPASS

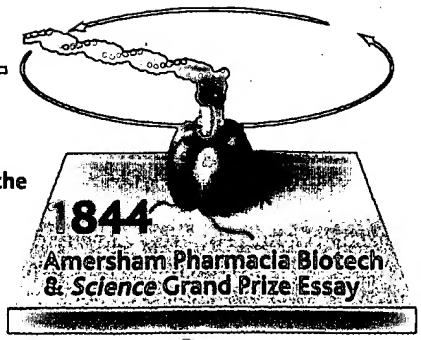

www.sciencemag.org/cgi/content/full/282/5395/1783a

1858
Trapped in the ice

Change of address: allow 4 weeks, giving old and new addresses and 8-digit account number. **Postmaster:** Send change of address to *Science*, P.O. Box 1811, Danbury, CT 06813–1811. **Single copy sales:** $7.00 per issue prepaid includes surface postage; bulk rates on request.

0026-895X/91/050756-10$03.00/0

MOLECULAR PHARMACOLOGY, 40:756-765

Frequency and Voltage-Dependent Inhibition of Type IIA Na^+ Channels, Expressed in a Mammalian Cell Line, by Local Anesthetic, Antiarrhythmic, and Anticonvulsant Drugs

DAVID S. RAGSDALE, TODD SCHEUER, and WILLIAM A. CATTERALL
Department of Pharmacology, University of Washington, School of Medicine, Seattle, Washington 98195
Received June 25, 1991; Accepted August 12, 1991

SUMMARY

This study examined the actions of phenytoin, carbamazepine, lidocaine, and verapamil on rat brain type IIA Na^+ channels functionally expressed in mammalian cells, using the whole-cell voltage-clamp recording technique. The drugs blocked Na^+ currents in both a tonic and use-dependent manner. Tonic block was more pronounced at depolarized holding potentials and reduced at hyperpolarized membrane potentials, reflecting an overall negative shift in the relationship between membrane potential and steady state inactivation. Dose-response relationships with phenytoin supported the hypothesis that the voltage dependence of tonic block resulted from the higher affinity of the drugs for inactivated than for resting channels. At −62 mV, approximately 50% of the Na^+ channels were blocked by phenytoin at 13 μM, compared with therapeutic brain levels of 4–8 μM. The use-dependent component of block developed progressively during a 2-Hz train of 40-msec-long stimulus pulses from −85 mV to 0 mV. At 2 Hz, verapamil was the most potent use-dependent blocker, lidocaine and phenytoin had intermediate potencies, and carbamazepine was least effective. The use-dependent block resulted from drug binding to open and inactivated channels during the depolarizing pulses and the slow repriming of drug-bound channels during the interpulse intervals. Verapamil, lidocaine, and phenytoin all bound preferentially to open channels, but this open channel block was most striking for verapamil. Use-dependent block was less pronounced at hyperpolarized membrane potentials, due to more rapid repriming of drug-bound channels. The results indicate that type IIA Na^+ channels expressed in a mammalian cell line retain the complex pharmacological properties characteristic of native Na^+ channels. These channels are likely to be an important site of the anticonvulsant action of phenytoin and carbamazepine. Lidocaine and verapamil, drugs with well characterized effects on peripheral Na^+ and Ca^{2+} channels, are also effective blockers of these brain Na^+ channels.

Voltage-gated Na^+ channels are large glycoproteins that form voltage-dependent, Na^+-selective pores through the membranes of excitable cells (1). At hyperpolarized membrane potentials, most Na^+ channels are in a closed resting state. The channels open in response to depolarization, resulting in inward Na^+ flux, and then rapidly convert to a nonconducting inactivated state. Repolarization of the membrane removes inactivation, converting the channels back to the resting state. The depolarization-activated ion flux through Na^+ channels plays a central role in the regenerative electrical properties of neurons and muscle cells.

The main functional component of the channel is the 260-kDa α subunit (2–5). Na^+ channels in rat brain also contain two smaller β subunits of 36 and 33 kDa, whereas Na^+ channels of rat skeletal and cardiac muscle contain a single β subunit of 38 kDa. Na^+ currents in neurons, cardiac cells, and skeletal muscle cells display different electrophysiological and pharmacological properties, and Na^+ channel subtypes with distinct primary structures are expressed in these tissues (6, 7). Four α subunit cDNAs (types I, II, IIA, and III), with >85% sequence identity, have been isolated from rat brain cDNA libraries (8, 9). Types II and IIA differ by only six amino acids. The α subunit alone forms a functional channel when expressed in *Xenopus* oocytes (8, 9), whereas the role of the β subunits is not known.

An increasing body of evidence indicates that a number of clinically important drugs exert their therapeutic effects principally by blocking Na^+ channels. For example, the anticonvulsants phenytoin and carbamazepine, which are effective against grand mal and partial seizures, are potent blockers of neuronal Na^+ channels at therapeutically relevant concentrations (10, 11). The local anesthetic lidocaine suppresses cardiac arrhythmias by blocking cardiac Na^+ channels (12) and is also an effective, although less potent, blocker of neuronal Na^+ channels (13). Verapamil, another effective antiarrhythmic, is believed to exert its effect principally by blocking cardiac Ca^{2+}

This work was supported by National Institutes of Health Research Grant NS15751 and a grant from the Parke-Davis Division, Warner-Lambert Co. (W.A.C.) and a postdoctoral research fellowship from National Institutes of Health (D.S.R.)

ABBREVIATIONS: CHO, Chinese hamster ovary; HEPES, 4-(2-hydroxyethyl)-1-piperazineethanesulfonic acid; EGTA, ethylene glycol bis(β-aminoethyl ether)-*N,N,N',N'*-tetraacetic acid.

channels (12), but it also blocks cardiac Na^+ channels (14). Na^+ channel block by verapamil is not well characterized but may be an important mechanism by which verapamil affects the excitability of cardiac cells. Verapamil and lidocaine also suppress epileptiform activity in brain neurons (15–18), perhaps by blocking brain Na^+ channels.

In voltage-clamp experiments, the blocking action of local anesthetics, anticonvulsants, and antiarrhythmics is greater at more depolarized holding potentials, and an additional "use-dependent" component of block accumulates during a train of stimulus pulses (12, 13, 19). The modulated receptor hypothesis (12, 13, 19) proposes that these characteristics reflect the higher affinity of local anesthetics, anticonvulsants, and antiarrhythmics for open and inactivated channels than for resting channels. Thus, use-dependent block during a train of pulses reflects the accumulation of drug binding to open and inactivated channels during each depolarizing pulse, whereas the dependence of block on holding potential reflects the predominance of inactivated channels at depolarized holding potentials and resting channels at hyperpolarized potentials. Neurons and cardiac cells in seizure and arrhythmic foci are typically more depolarized than normal cells and fire rapid bursts of action potentials. Thus, the use- and voltage-dependence of anticonvulsant and antiarrhythmic block may explain the ability of these drugs to selectively suppress the abnormal cell electrical activity that is responsible for seizures and arrhythmias, while not appreciably altering normal cell activity (10, 12).

The functional role and pharmacological significance of the different Na^+ channel subtypes is not clear. The type I and II channels are heterogeneously distributed in the rat brain (20, 21) and are localized to specific regions of individual neurons (22). They are not expressed at high levels in peripheral neurons. Determining the pharmacological properties of Na^+ channels expressed from single α subunit cDNAs and characterizing the relative effects of local anesthetics, anticonvulsants, and antiarrhythmics on the Na^+ channels encoded by different α subunit subtypes will be important steps in understanding the clinical effects of these drugs. Na^+ currents expressed in oocytes injected with RNA from α subunit cDNAs inactivate abnormally slowly, compared with Na^+ currents in mammalian neurons (9). Thus, for Na^+ channels, results obtained from oocytes must be interpreted with caution. We have recently developed a mammalian cell line, called CNaIIA-1, that has been stably transfected with cDNA encoding the type IIA subtype of the Na^+ channel α subunit and expresses high levels of functional type IIA Na^+ channels. These channels have electrophysiological characteristics that are similar to those seen in mammalian neurons (23, 24). In this study, we have used whole-cell voltage-clamp recording to characterize the effects of the anticonvulsants phenytoin and carbamazepine and the antiarrhythmics lidocaine and verapamil on the rat brain Na^+ channels expressed in CNaIIA-1 cells. Our results provide a more detailed characterization of the effects of these drugs on brain sodium channels than has been possible with previous physiological preparations.

Materials and Methods

Cell culture. All experiments were performed using the cell line CNaIIA-1, which was derived from a CHO cell line (CHO-K1; American Type Cultures) transfected with the vector ZEM2580 containing a cDNA encoding the rat brain type IIA Na^+ channel. The rat IIA sequence used contains the natural leucine at position 860, conferring normal voltage-dependent properties (25). The vector places the Na^+ channel cDNA under the control of the mouse metallothionein promoter. The vector also contains a neomycin resistance gene, which confers resistance to the antibiotic G418. A more detailed description of cloning of the type IIA Na^+ channel and its transfection into CHO cells is given elsewhere (9, 23–25).

CNaIIA-1 cells were cultured in 35-mm plastic Petri dishes in RPMI medium (GIBCO) with 10% fetal calf serum and streptomycin (2 mg/ml) and penicillin (4 mg/ml) to inhibit microbial growth. G418 was also included to select for transfectants. The cells were grown either directly on the bottom of the Petri dishes or on pieces of glass coverslips in the dishes.

Electrophysiology. Electrophysiological recording was performed either with the whole Petri dishes or with pieces of glass coverslips transferred to a 200-μl recording chamber. The culture medium was replaced by an extracellular recording solution containing (in mM) NaCl, 130; KCl, 5.0; $CaCl_2$, 1.5; $MgCl_2$, 1.0; glucose, 5.0; and HEPES, 5.0; pH 7.4 with NaOH. All recordings were at room temperature (~20–22°).

Na^+ currents were recorded using the whole-cell configuration of the patch-clamp recording technique (26). Recording pipettes were pulled from hematocrit microtubes and back-filled with an intracellular solution containing (in mM) CsF, 90; Cs-EGTA, 10; CsCl, 60; NaF, 10; and HEPES, 10; pH 7.4 with CsOH. The pipettes had input resistances of ~1–2 MΩ. The cells were clamped using a conventional patch-clamp amplifier (List L/M EPC-7). Data acquisition and analysis were performed with a personal computer, using commercially available software (Basic-Fastlab, Indec Systems). The data were filtered at 10 kHz, digitized, and stored on the computer hard disk. Theoretical curves were fit to the data using a least squares algorithm (27). Series resistance and capacitive transients arising from voltage steps were compensated using the internal clamp circuitry. In some cases, the remaining capacitive currents and leak currents were subtracted by the $P/4$ subtraction procedure (28). The settling time of the clamp before series resistance compensation was <100 μsec. The series resistance in the whole-cell configuration was approximately 3 mΩ; 70–75% of the series resistance was compensated. We estimate that, for typical Na^+ currents of 2–5 nA, the voltage drop across the series resistance was <4 mV.

Drug application. Stock solutions (20 mM) of phenytoin, carbamazepine, lidocaine, and verapamil were prepared in dimethyl sulfoxide and then diluted into the recording solution to the desired concentrations for experiments. Control recordings showed that 1.0% dimethyl sulfoxide, the highest concentration used in any experiment, had no detectable effects on the Na^+ currents in CNaIIA-1 cells. For the dose-response curves and some other experiments, the drugs were applied by superfusion; however, it was difficult to maintain gigaseals on CNaIIA-1 cells with this technique. Thus, for most experiments drugs were applied by adding the appropriate volume of stock solution directly to the bath and then gently mixing the drug into the bath for about 5 min. There were no obvious differences in the drug effects using these two methods, and we were able to routinely record from cells for >1 hr by directly adding the drugs to the bath.

Results

Effects of anticonvulsants and antiarrhythmics on Na^+ currents. Depolarization of CNaIIA-1 cells from −85 to 0 mV evoked transient inward currents that inactivated within a few milliseconds, were blocked by tetrodotoxin, and reversed around the Na^+ equilibrium potential. Thus, the currents were due to activation of voltage-gated Na^+ channels. Untransfected CHO cells display little inward current under the same recording conditions (23, 24), indicating that the Na^+ channels expressed in CNaIIA-1 cells were encoded by the transfected cDNA, rather than being native to the cell line.

Fifty micromolar phenytoin, carbamazepine, lidocaine, and verapamil all rapidly reduced the amplitude of the Na^+ currents evoked by infrequently applied stimulus pulses (i.e., ≤0.05 Hz),

without having any obvious effects on their time course (Fig. 1, *curves A* and *B*). Verapamil was the most potent blocker, typically reducing Na^+ currents by 60–80% (Table 1). Phenytoin and carbamazepine were somewhat less effective, reducing Na^+ currents by 20–40%, whereas lidocaine was the least potent tonic blocker, reducing the currents by ~10%.

In addition to this tonic block, the antagonists also inhibited Na^+ currents in a use-dependent manner. Thus, the amplitude of the Na^+ currents became progressively smaller during a 2-Hz train of depolarizing pulses in the presence of the blockers (Fig. 1, *curve C*). As with tonic block, there was considerable variability in the potency of the different drugs for use-dependent block. Verapamil was the most effective, whereas lidocaine and phenytoin had intermediate potencies and carbamazepine was relatively ineffective (Table 1). Both tonic and use-dependent block displayed complex properties, which we characterized in more detail, as described below.

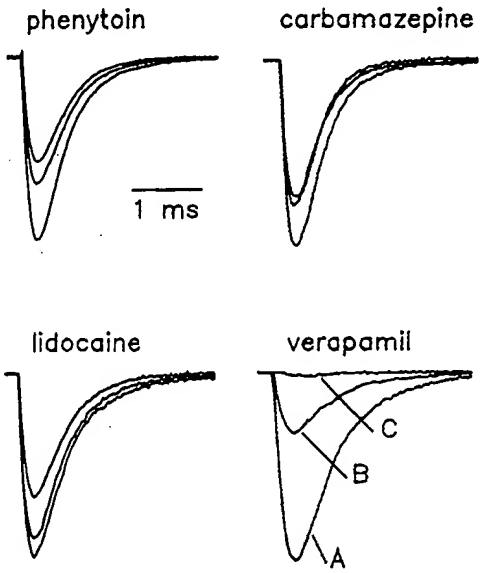

Fig. 1. Tonic and use-dependent block of Na^+ currents in CNaIIA-1 cells by phenytoin, carbamazepine, lidocaine, and verapamil. The cells were held at a membrane potential of −85 mV, and Na^+ currents were evoked by applying stimulus pulses to 0 mV. Each set of current traces is from a single cell and shows currents elicited by stimulus pulses in control conditions (*curve A*), about 5 min after the drugs were washed on (*curve B*), and by the 20th pulse in a train of repetitive, 40-msec-long pulses, at a frequency of 2 Hz (*curve C*). In this and subsequent figures, the drug concentrations were 50 μM, unless stated otherwise. Note that the current records were normalized so that the control currents for each cell are the same size. The amplitudes of the control currents actually ranged from about 3 to 6 nA.

Characterization of tonic block of Na^+ currents by local anesthetics, anticonvulsants, and antiarrhythmics. To examine whether tonic block reflected altered activation or permeability properties of Na^+ channels in CNaIIA-1 cells, we determined current-voltage relationships in control conditions (i.e., in normal bath solution) and then in the presence of the blockers (Fig. 2). From a prepulse potential of −100 mV, inward Na^+ currents were just detectable with depolarizations to approximately −50 mV. The peak Na^+ currents were maximal at around 0 mV, and the currents became outward at depolarizations more positive than about +65 mV, which corresponds to the Na^+ equilibrium potential with the internal and external recording solutions used in these experiments. In the presence of blockers, the currents were smaller at all test potentials, and there were no changes in the activation properties or reversal potential of the currents. The effects of the drugs were partially reversible during washout for as long as stable seals could be maintained. Fig. 2 shows a typical experiment with phenytoin. Similar results were obtained with carbamazepine, lidocaine, and verapamil.

One of the most striking features of tonic block was its strong dependence on the holding membrane potential of the cells. For example, 50 μM phenytoin reduced Na^+ currents by <10% in cells depolarized to 0 mV from a holding potential of −128 mV, but the currents were reduced by >90% when the holding potential was −66 mV (Fig. 3). Carbamazepine, lidocaine, and verapamil were also more potent blockers at more positive holding potentials. This potential-dependence is similar to previous findings (10–13, 19). According to the modulated receptor model, potential-dependence stems from the higher affinity of the drugs for inactivated than for resting channels, resulting in an overall negative shift in the relationship between membrane potential and steady state inactivation.

We investigated the effects of anticonvulsants and antiarrhythmics on steady state inactivation in more detail by determining complete steady state inactivation curves in the absence and presence of drugs, using two different experimental proto-

TABLE 1

Summary of drug effects on rat brain type IIA Na^+ channels expressed in cultured mammalian cells

	Tonic block[a]		Use-dependent block[b]	h_∞ shift (1-min prepulses)[c]	Channel repriming[d]	
	V_m = −85 mV	V_m = −128 mV			τ_1	τ_2
	%		%	mV	msec	
Phenytoin	28.1 ± 3.6 (n = 9)	13.9 ± 6.0 (n = 4)	19.9 ± 1.5 (n = 6)	−9.50 ± 0.40 (n = 4)	7.22 ± 0.60 (n = 3)	150.60 ± 39.34 (n = 3)
Carbamazepine	28.3 ± 4.5 (n = 6)	6.8 ± 3.4 (n = 3)	8.1 ± 1.8 (n = 5)	−6.13 ± 0.73 (n = 4)	7.60 ± 0.31 (n = 2)	52.91 ± 2.78 (n = 2)
Lidocaine	8.6 ± 3.2 (n = 7)	2.4 ± 1.4 (n = 3)	27.8 ± 2.4 (n = 5)	−7.35 ± 1.47 (n = 3)	11.63 ± 0.63 (n = 3)	667.00 ± 62.12 (n = 3)
Verapamil	72.9 ± 3.5 (n = 8)	32.4 ± 16.7 (n = 3)	79.1 ± 8.6 (n = 6)	−16.14 ± 1.91 (n = 3)	8.67 ± 0.97 (n = 2)	5234.50 ± 390.66 (n = 2)
Control			6.7 ± 1.0 (n = 17)		5.08 ± 0.25 (n = 11)	

[a] The experimental protocol is described in Fig. 1. Data are presented as mean ± standard error and show the percentage of inhibition of the peak currents in the presence of a 50 μM concentration of each drug.

[b] The protocol is described in Fig. 7. The data show the percentage of inhibition of the current evoked by the 20th pulse in a 2-Hz train, compared with the current evoked by the first pulse.

[c] The protocol is described in Fig. 5.

[d] The protocol is described in Fig. 11.

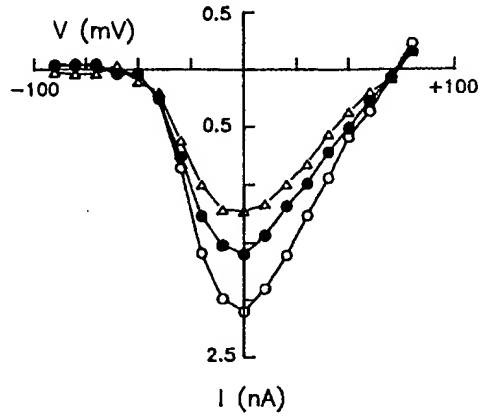

Fig. 2. Effects of phenytoin on the voltage dependence of Na^+ channel activation. The data are from a representative cell in control conditions (○), in the presence of phenytoin (△), and about 10 min after washing out the drug (●). The current-voltage relationships were determined by application of 100-msec prepulses to −95 mV, followed by test pulses to potentials ranging from −85 to +76 mV. The pulses were applied every 3 sec, and the cells were held at −76 mV between stimuli. The amplitudes of the peak currents were plotted as a function of test pulse potential.

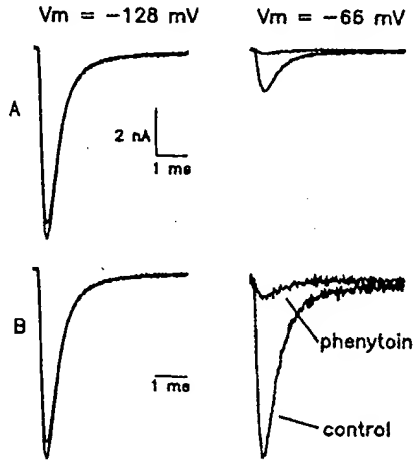

Fig. 3. Effects of holding potential on tonic block of Na^+ currents by phenytoin. The records are from a single representative cell. A, Na^+ currents were evoked by pulsing to 0 mV, from holding potentials of −128 mV (*left*) or −66 mV (*right*), without a prepulse in control conditions and then in the presence of phenytoin. B, The same traces were normalized so that the control currents at −128 and −66 mV are the same size.

cols. In the initial experiments, inactivation was assessed by the amplitude of the currents elicited by a test pulse to 0 mV after a 100-msec prepulse to various potentials. Fig. 4 shows a typical result for phenytoin. The smooth curve through the control data is according to the equation:

$$1/(1 - \exp((E - E_h)/k)) \quad (1)$$

where E = membrane potential, E_h = the prepulse potential where the current is half-maximal, and k = the slope factor. In the presence of drugs, there were relatively small (typically 1–5-mV) negative shifts in the midpoints of the inactivation curves determined in this way. In addition, the inactivation curves in the presence of the drugs had more shallow slopes than control curves, did not reach a plateau at very negative prepulse potentials, and were not well fit by Eq. 1. This probably indicated that, in the presence of the drugs, the 100-msec prepulses were not long enough to reach a steady state at a

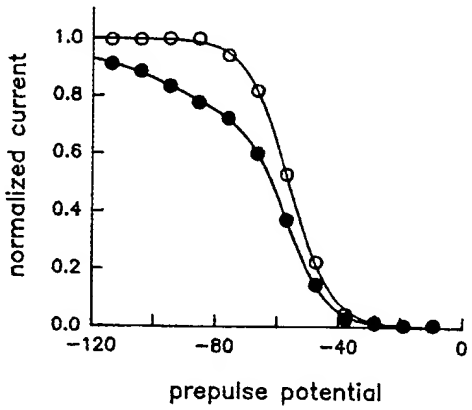

Fig. 4. Effect of phenytoin on the voltage dependence of Na^+ channel inactivation, determined using short prepulses. The data are from a representative cell in control conditions (○) and in the presence of 50 μM phenytoin (●). The fraction of available channels as a function of membrane potential was assessed by application of 100-msec prepulses to potentials from −120 to −10 mV, followed by test pulses to 0 mV. Pulses were applied every 3 sec, and the cell was held at a membrane potential of −76 mV between stimuli. The data were normalized with respect to the amplitude of the current evoked in control conditions after a prepulse to −120 mV. The *smooth curve* through the control data is according to Eq. 1, with $h_{1/2}$ = −56.23 mV and k = 6.73.

given prepulse potential (see below), perhaps due to slowed transitions of drug-bound channels. Thus, to obtain a true steady state measure of the voltage dependence of inactivation in the absence and presence of drugs, the cells were held at various potentials for 1 min, followed by a test pulse to 0 mV. Using this procedure, the shifts in half-inactivation for phenytoin, carbamazepine, lidocaine, and verapamil were approximately −10, −6, −7, and −16 mV respectively (Fig. 5; Table 1). In addition, the inactivation data in the presence of the drugs reached a plateau at negative holding potentials and were well fit by Eq. 1, suggesting that these results were obtained under steady state conditions. Interestingly, there was still significant block with phenytoin, carbamazepine, and verapamil that was constant between holding potentials of about −100 to −128 mV (Fig. 5; Table 1), suggesting that these drugs blocked some resting channels at a concentration of 50 μM.

To examine more directly the difference in affinity of the drugs for resting and inactivated channels, we determined dose-response relationships for phenytoin at holding potentials of −85 mV, where most channels were in the resting state in control conditions, and −62 mV, where more than half the channels were inactivated in control recordings. A typical result from a single cell is shown in Fig. 6. At −85 mV, block of the Na^+ current was just detectable at 10 μM, and even at 100 μM the current was blocked by <50%. The Hill coefficient of the best fit line through the data points was 0.92, and the approximate EC_{50} determined by extrapolation of the best fit line was 162 μM. In contrast, at −62 mV, 1 μM phenytoin reduced the currents by about 10%, and at 100 μM the currents were almost completely blocked. The EC_{50} for phenytoin at −62 mV was 10 μM, and the Hill slope was 0.72. Similar results were obtained in two other cells; the EC_{50} values for all cells were 12.6 ± 3 μM (mean ± standard error) at −62 mV and 195 ± 71 μM at −85 mV.

Use-dependent block with anticonvulsants and antiarrhythmics. Fig. 7 shows the amplitudes of the currents evoked by a train of 20 pulses from −85 to 0 mV, in control conditions and in the presence of 50 μM phenytoin, carbamazepine, lido-

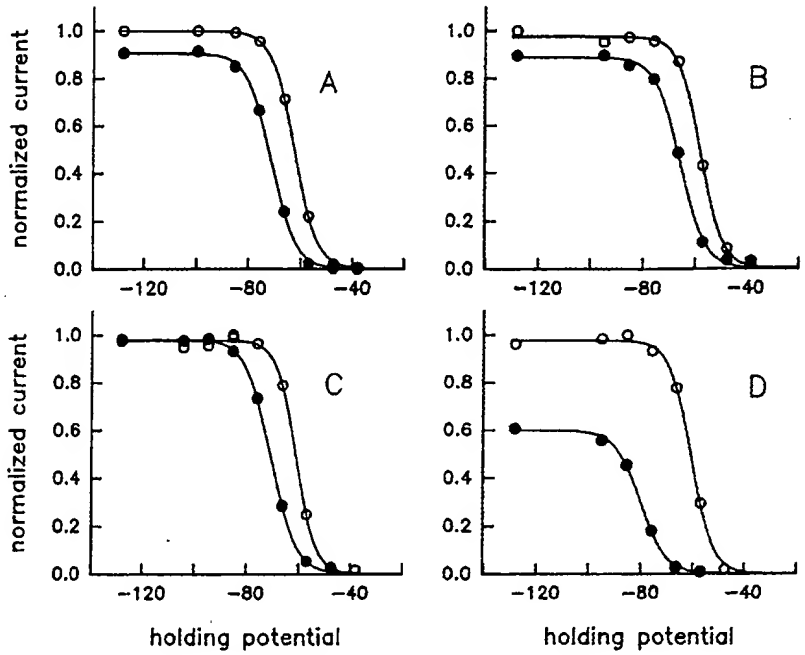

Fig. 5. Drug effects on the voltage dependence of steady state Na^+ channel inactivation. Each graph shows data from a single cell in control conditions (○) and after addition of one of the drugs at 50 μM (●), i.e., phenytoin (A), carbamazepine (B), lidocaine (C), or verapamil (D). The relationship between steady state inactivation and holding potential was determined by holding the cells for 1 min at membrane potentials ranging from −128 to −38 mV and then applying test pulses to 0 mV. The data were normalized with respect to the amplitude of the currents evoked from −128 mV in control conditions. The smooth curves are according to Eq. 1, with the following values for $h_{1/2}$ and k: A, control: $h_{1/2} = -62.50$ mV, $k = 4.32$; phenytoin: $h_{1/2} = -71.30$ mV, $k = 4.62$; B, control: $h_{1/2} = -57.89$ mV, $k = 4.23$; carbamazepine: $h_{1/2} = -65.73$, $k = 4.78$; C, control: $h_{1/2} = -61.04$ mV, $k = 3.77$; lidocaine: $h_{1/2} = -70.76$, $k = 4.86$; D, control: $h_{1/2} = -60.71$, $k = 4.24$; verapamil: $h_{1/2} = -80.10$ mV, $k = 4.90$.

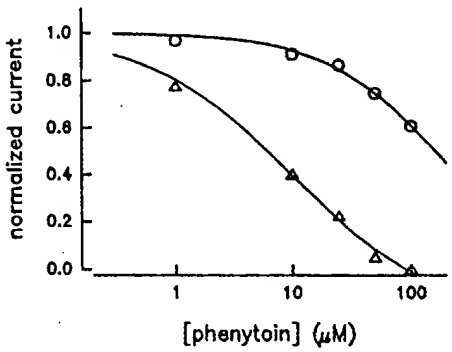

Fig. 6. Dose-response relationship for phenytoin at two different holding potentials. The data are from a representative cell. The drug concentration was varied from 1 to 100 μM by superfusion. Na^+ currents were evoked by pulsing to 0 mV from holding potentials of −85 mV (○) and −62 mV (△). The data were normalized with respect to the amplitudes of the currents evoked under control conditions at each holding potential. The smooth curves are according to the formula $1 - (1/(1 + (EC_{50}/[\text{drug}])^n))$, with $EC_{50} = 162$ and 10 μM and $n = 0.92$ and 0.72 for holding potentials of −85 and −62 mV, respectively.

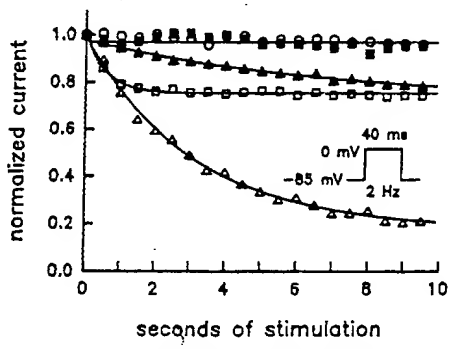

Fig. 7. Use-dependent block of Na^+ currents. The data points are from different cells in the presence of phenytoin (▲), carbamazepine (■), lidocaine (□), or verapamil (△). An example of typical control data is also shown (○). The cells were held at −85 mV, and Na^+ currents were elicited by trains of 20 stimulus pulses to 0 mV, at a frequency of 2 Hz. The duration of the pulses was 40 msec. For each experiment, the current amplitudes were normalized with respect to the current evoked by the first pulse in the train.

caine, and verapamil. The stimulus frequency was 2 Hz and the duration of each pulse was 40 msec. In the control recording, there was a small steady decline in the current amplitude. This use-dependent "droop" was usually ~5% by the 20th pulse in the train. In the presence of phenytoin, lidocaine, and verapamil, there was an additional decline in the currents, due to the accumulation of use-dependent block. The effect was clearly most pronounced with verapamil, where the currents typically declined to 10–30% of those in the first pulse by the end of the pulse train (Table 1). Lidocaine was the next most potent use-dependent blocker. With lidocaine, currents declined in the first few pulses to a steady state amplitude that was ~65–75% of the current evoked by the first pulse in the train. Use-dependent block developed more slowly with phenytoin, and by the 20th pulse in the train Na^+ currents were about 80% of the first pulse. Carbamazepine at a stimulus frequency of 2 Hz displayed virtually no use-dependent block.

The extent of use-dependent block increased with increasing frequency, and there were differences among the drugs in the stimulus frequency at which use-dependent block became clearly detectable (Fig. 8). From a holding potential of −85 mV, stimulus frequencies of about 4 Hz were necessary to clearly observe use-dependent block with 50 μM carbamazepine, whereas 50 μM phenytoin and lidocaine blocked Na^+ currents in a use-dependent manner with stimulus frequencies greater than or equal to about 1 and 0.5 Hz, respectively. The most striking effects were with 50 μM verapamil, where use-dependent block was present at frequencies as low as four pulses/min (0.067 Hz).

Rates of drug association. The accumulation of use-dependent block during a train of stimulus pulses results from the association of the drugs to open and inactivated channels during each depolarizing pulse and the relatively slow recovery of drug-bound channels during the interpulse intervals. To determine whether the large differences in use-dependent block seen with the different blockers reflected differences in either the association or recovery kinetics, we investigated the kinetics of use-dependent block in more detail.

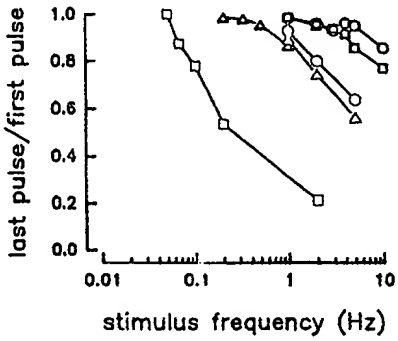

Fig. 8. Extent of use-dependent block at different stimulus frequencies. The data were obtained from five different cells in the presence of phenytoin (○), carbamazepine (□), lidocaine (△ and △, representing two different cells), or verapamil (□). Typical control data are also shown (○) (same cell as for carbamazepine). At each frequency, stimulus pulses were applied until the use-dependent block was approximately at steady state. The graph shows the ratio of the amplitudes of the currents evoked by the last pulse in the train divided by the currents evoked by the first pulse in the train, plotted as a function of stimulus frequency.

The rate of drug association was examined by applying a conditioning pulse to 0 mV for varying durations (from 1 to 100 msec), followed by a recovery prepulse to −85 mV for 30 msec and then a test pulse to 0 mV. The fraction of channels that bound drug during the conditioning pulse was determined by taking the ratio of peak Na^+ currents evoked by the test pulse and the conditioning pulse. The recovery interval was chosen to be short enough to "catch" most of the drug-bound channels before the drug dissociated but long enough for complete repriming of unbound channels (see below).

The results indicated that there were differences in the kinetics of association for the different drugs (Fig. 9). With 50 μM phenytoin, carbamazepine, and lidocaine, there was a small rapid component of block with conditioning pulse durations up to 2 msec (Fig. 9, *right*), and then the extent of block increased steadily as the pulse duration was increased up to 100 msec (Fig. 9, *left*). With 100 and 200 μM lidocaine and phenytoin, the overall extent of block was greater, and the initial rapid component was more pronounced. The rapid component of block corresponded to the brief period when most Na^+ channels were open (see the current traces above the panels in Fig. 9). These results indicate that the biphasic time course of association of these drugs resulted from rapid binding to open or partially activated channels, followed by slow binding to inactivated channels. Phenytoin, carbamazepine, and lidocaine bound significantly to both open and inactivated channels. However, because the channel open time was so brief, the use-dependent block shown in Fig. 7 was probably due primarily to drug binding to inactivated channels. In fact, use-dependent block was strongly dependent on pulse duration far beyond the time during which channels were open. When tested with trains of stimulus pulses of variable duration, with the interpulse interval maintained constant at 500 msec, no use-dependent block was seen with phenytoin or lidocaine during pulse trains of 4 msec or less (Fig. 10). Increased use-dependent block was observed for pulse durations of 20, 40, and 100 msec for these drugs, even though the channels were open only during the first 3 msec.

The time course of association for verapamil was clearly different from that for the other drugs. With 50 μM verapamil, the extent of block increased rapidly for pulse durations up to 2 msec and then increased much more gradually as the pulse duration was further increased up to 100 msec (Fig. 9). When the verapamil concentration was increased to 100 μM, the extent of the rapid block was approximately doubled, but the slower component seen at longer pulse durations was essentially unchanged. These results indicate that verapamil bound rapidly to open channels and much more slowly to inactivated channels. Consistent with this, in the presence of 50 μM verapamil dramatic use-dependent block was seen with stimulus pulses as short as 0.6 msec, and the extent of block increased substantially for stimulus pulses of 1 msec (Fig. 10). In contrast, the increment in use-dependent block observed when the pulse duration was increased from 1 msec to 20, 40, and 100 msec was modest, indicating a less important role for binding to inactivated channels in the use-dependent block by verapamil. (Fig. 10).

Rates of drug dissociation. The rate of channel recovery from inactivation was examined by application of a 100-msec conditioning pulse to 0 mV, followed by a recovery pulse to −85 mV for varying durations and then a test pulse to measure the extent of channel repriming. In control conditions, the rate of recovery was well fit by a single exponential function with a time constant of about 4–6 msec (Fig. 11; Table 1). Recovery was essentially complete within 30 msec. In the presence of 50 μM phenytoin, carbamazepine, lidocaine, or verapamil, recovery had two distinct components and was well fit by the sum of two exponentials. The time constant for the fast component was typically around 6–12 msec, whereas the time course of the slow component depended on which drug was present, i.e., about 50 msec for carbamazepine, 100–200 msec for phenytoin, 600–700 msec for lidocaine, and 5 sec for verapamil (Table 1). Presumably, the rapid component of recovery reflected the rapid recovery of channels that did not bind drug during the conditioning pulse, whereas the slow component of repriming reflected the relatively slow recovery of drug-bound channels. The large difference in the rate of the slow recovery for the different drugs was the main factor determining their potencies as use-dependent blockers.

It has previously been shown that recovery of both unbound and drug-bound Na^+ channels is faster at hyperpolarized membrane potentials (12). Consistent with this, we found that, for phenytoin, lidocaine, and verapamil, use-dependent block was less when stimulus pulses were applied from a holding potential of −128 mV, compared with a holding potential of −85 mV (Fig. 12). The dependence of recovery on membrane potential was also more directly examined with lidocaine, using the two-pulse protocol described in Fig. 10, with recovery prepulses to −85 mV and −128 mV (Fig. 13). In control conditions, the time constants of recovery at −85 mV and −128 mV were 5.5 and 1.0 msec, respectively. Thus, recovery from inactivation was about 5 times faster at −128 mV than at −85 mV. In the presence of 50 μM lidocaine, the fast component of recovery had time constants of 10.9 and 1.6 msec at −85 and −128 mV, whereas the slow component of recovery had time constants of 775 and 136 msec. Thus, lidocaine-bound channels also recovered more rapidly at −128 mV than at −85 mV.

Discussion

Inhibition of type IIA Na^+ channel α subunits by local anesthetic, antiarrhythmic, and anticonvulsant drugs, in a frequency- and voltage-dependent manner. A major finding of this study is that local anesthetic, antiarrhythmic, and anticonvulsant drugs block cloned rat brain type IIA Na^+

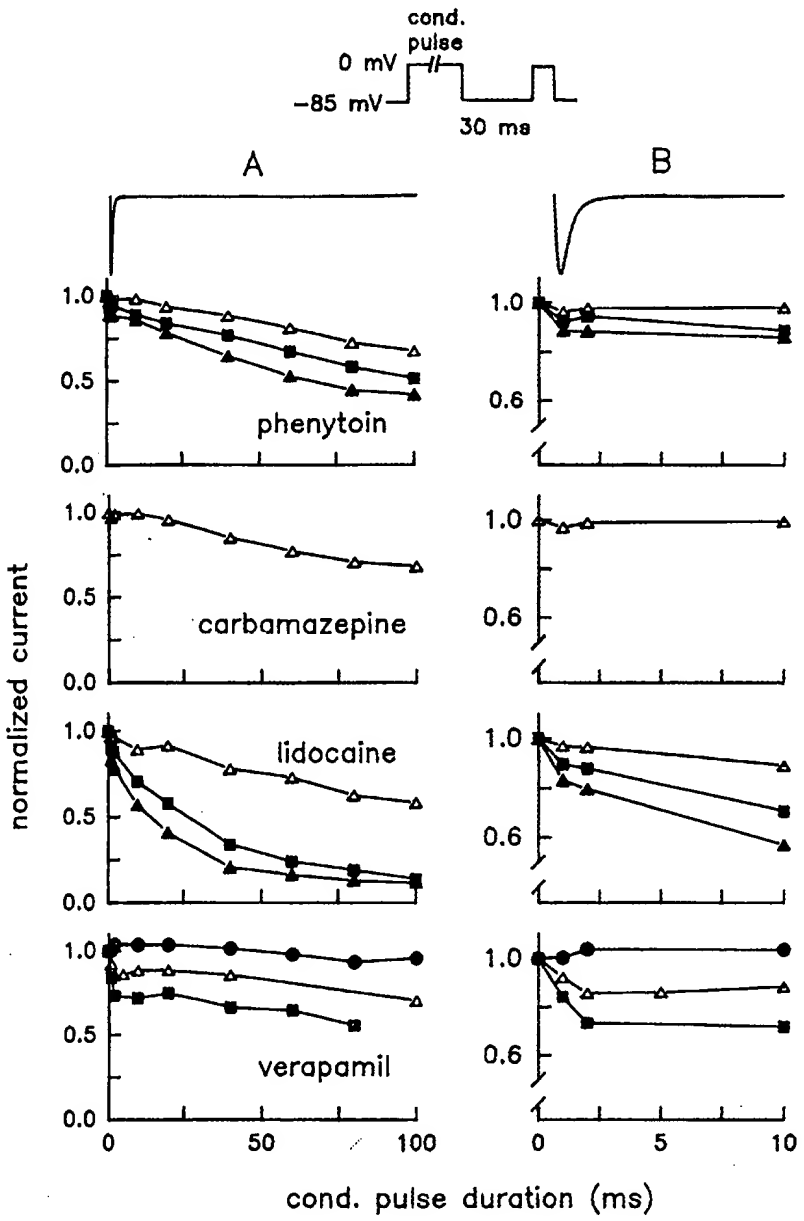

Fig. 9. Rate of development of drug block during depolarization. The data were obtained in the presence of phenytoin, carbamazepine, lidocaine, or verapamil, at concentrations of 50 (△), 100 (■), or 200 (▲) μM. The data for phenytoin, lidocaine, and verapamil were from two different cells for each drug (designated by *open* and *filled symbols*). The graph for verapamil also shows typical control data (●). A, Development of drug block was assessed by application of a conditioning pulse to 0 mV, of variable duration (1–100 msec), followed by a 30-msec recovery interval to −85 mV and then a test pulse to 0 mV. The amplitudes of the currents evoked by the test pulse were normalized with respect to the currents elicited by the conditioning pulse and are plotted as a function of conditioning pulse duration. B, The same data, showing conditioning pulses up to 10 msec on an expanded time scale. *Traces above each column*, typical Na^+ currents, during depolarizations to 0 mV, on the same time scales as the respective graphs.

channel α subunits, expressed in a heterologous mammalian cell line, in a manner that is dependent on holding potential and frequency of stimulation, as for native sodium channels. The results indicate that these drugs bind with higher affinity to open and inactivated channels than to resting channels. They are consistent with extensive previous studies of frequency- and voltage-dependent block of Na^+ channels in neurons and cardiac myocytes (10–13, 19). Assuming that CHO cells do not express endogenous Na^+ channel β subunits, the results show that the α subunit alone is responsible for the characteristic pharmacological interactions between Na^+ channels and local anesthetics, antiarrhythmics, and anticonvulsants. The preparation used in this study presents important experimental advantages, because it consists of a homogeneous population of a known rat brain Na^+ channel subtype expressed in a cell line that has low endogenous levels of Na^+, Ca^{2+}, and K^+ channels and is amenable to high resolution whole-cell voltage-clamp recording techniques. These favorable characteristics have allowed us to make a more complete study of the interactions of these drugs with brain sodium channels than was possible previously.

Inhibition of type IIA Na^+ channels as an anticonvulsant mechanism. The findings for phenytoin and carbamazepine are directly relevant to their pharmacological actions, because these drugs are thought to exert their anticonvulsant effects mainly by blocking brain Na^+ channels (10, 11). Typical therapeutic concentrations for these drugs in the cerebrospinal fluid are about 3–8 μM (10, 11). Although 10 μM phenytoin (approximately the therapeutic cerebrospinal fluid concentration) had little effect on Na^+ currents in CNaIIA-1 cells held at −85 mV, it strongly blocked currents when the holding potential was −62 mV. Thus, at clinically relevant concentrations, phenytoin blocked Na^+ currents mediated by type IIA α subunits at the relatively positive resting membrane potentials characteristic of neurons during seizure activity, but not at the more hyperpolarized resting membrane potentials typical of neurons during normal cell activity. These results are similar to those of previous drug binding, ion flux, and electrophysiological studies, in which phenytoin and carbamazepine were shown to bind to and inhibit Na^+ channels in mammalian neurons at therapeutically relevant concentrations (29–34).

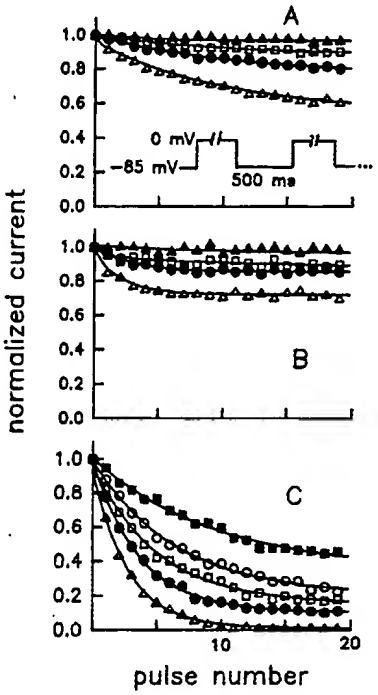

Fig. 10. Effect of pulse duration on use-dependent block. Each graph shows data from a single cell, with phenytoin (A), lidocaine (B), or verapamil (C). The cells were held at −85 mV, and Na^+ currents were evoked by a train of 20 stimulus pulses to 0 mV. The durations of the pulses were 4 (▲), 20 (□), 40 (●), and 100 (△) msec for A and B and 0.6 (■), 1 (○), 20 (□), 40 (●), and 100 (△) msec for C. The duration of the interpulse interval was held constant at 500 msec. The data were plotted as described in Fig. 7.

The voltage dependence of drug binding presumably explains, at least in part, the ability of phenytoin to block seizures without affecting normal brain function (10, 11, 32).

Neither phenytoin nor carbamazepine was a potent use-dependent blocker of type IIA Na^+ channels at a stimulus frequency of 2 Hz. However, use-dependent block with these drugs became more pronounced at higher stimulus frequencies. These use-dependent effects may be important for filtering the high frequency bursts of action potentials characteristic of epileptiform activity.

Type I and II/IIA Na^+ channels account for >85% of adult brain Na^+ channels in the rat but are not highly expressed in peripheral neurons or peripheral nerves (20). Type II/IIA Na^+ channels are preferentially localized in axons of central neurons (22). They may be responsible for initiation of the conducted action potential at the axon initial segment and conduction along the axon. Our results imply that both initiation and propagation of action potentials in central neurons would be inhibited by phenytoin and carbamazepine. Type I Na^+ channels are localized primarily in the cell bodies of major projection neurons in the brain (22). It will be of interest in the future to compare the actions of anticonvulsant drugs on type I and type IIA Na^+ channels expressed in a mammalian cell line.

Lidocaine and verapamil also have anticonvulsant properties (15–18); however, it is not clear whether either of these drugs would be clinically useful for treating seizures. In at least one case, lidocaine suppressed seizures in a human epileptic after more conventional anticonvulsants had proven ineffective (16). Thus, lidocaine may have some utility. However, verapamil, at concentrations sufficiently high to inhibit seizures, would have undesired side effects, due to its actions on peripheral Ca^{2+} channels. It, therefore, would probably not be a clinically useful anticonvulsant, even if it crossed the blood-brain barrier effectively.

Characterization of frequency- and voltage-dependent drug effects. The strong voltage dependence of block by the local anesthetics, anticonvulsants, and antiarrhythmics studied here reflected an overall negative shift in the relationship between steady state inactivation and membrane potential. The time constants for Na^+ channel inactivation in various cell types are typically a few milliseconds and, therefore, experimental protocols that assess steady state inactivation usually use relatively short (e.g., 100-msec) prepulses, followed by a test pulse to measure the ratio of resting and inactivated channels. However, in this study 100-msec prepulses were too

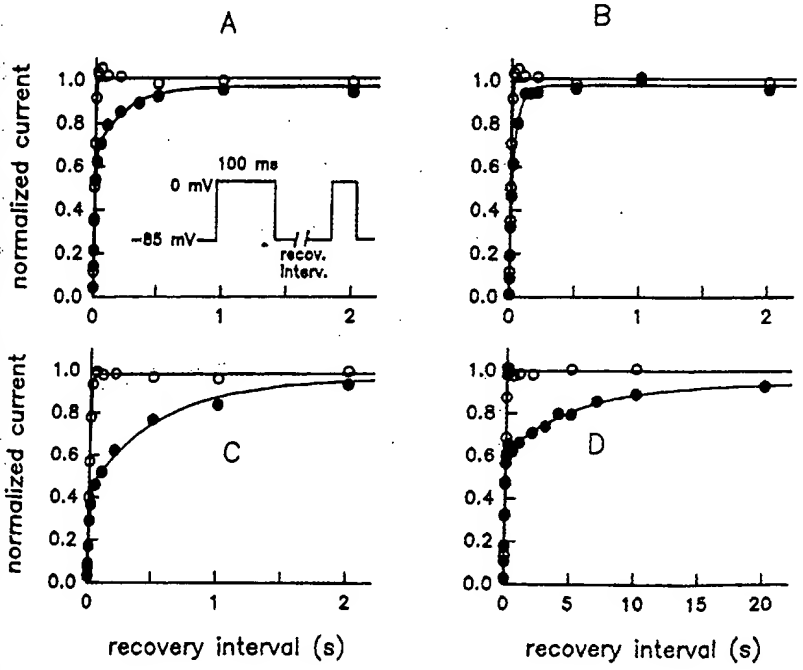

Fig. 11. Drug-induced slowing of Na^+ channel recovery. The graphs show data from four cells in control conditions (○) and after addition of 50 μM levels of the indicated drug (●), i.e., phenytoin (A), carbamazepine (B), lidocaine (C), or verapamil (D). The extent of channel repriming was determined by applying 100-msec conditioning pulses to 0 mV and then stepping to −85 mV for varying durations, followed by test pulses to 0 mV. The amplitudes of the currents evoked by the test pulses were normalized with respect to the currents elicited by the conditioning pulses and are plotted as a function of the recovery interval. The *smooth lines* through the control data are according to the equation $1 - \exp(-t/\tau)$, where t is recovery interval and τ = 5.20, 5.86, 6.13, and 4.72 msec for A, B, C, and D, respectively. The data in the presence of drugs were fit by $1 - (c_1 \exp(-t/\tau_1) + c_2 \exp(-t/\tau_2))$, with τ_1 = 7.17, 7.27, 11.03, and 7.69 msec and τ_2 = 228.6, 55.6, 559.8, and 5624.0 msec for A, B, C, and D, respectively. Note the different time scale for D.

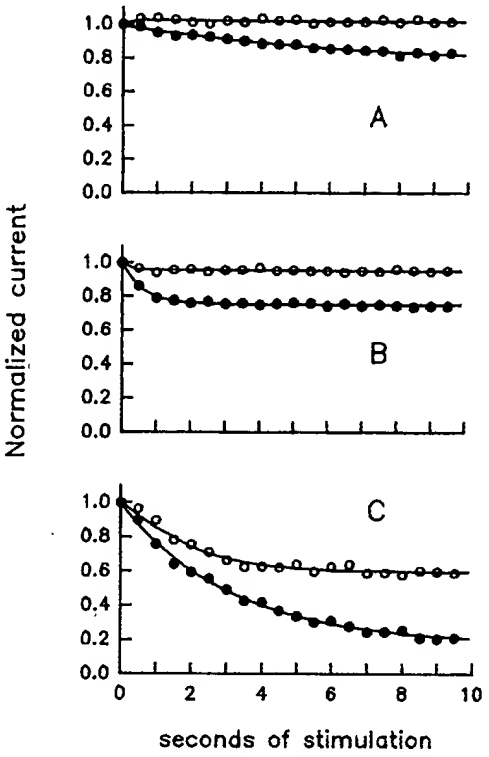

Fig. 12. Effect of holding potential on use-dependent block. Each graph shows data from a single cell, with phenytoin (A), lidocaine (B), or verapamil (C). A 2-Hz train of 40-msec-long pulses was applied from holding potentials of −128 (○) and −85 (●) mV. Current amplitudes were normalized with respect to the first pulse of the train.

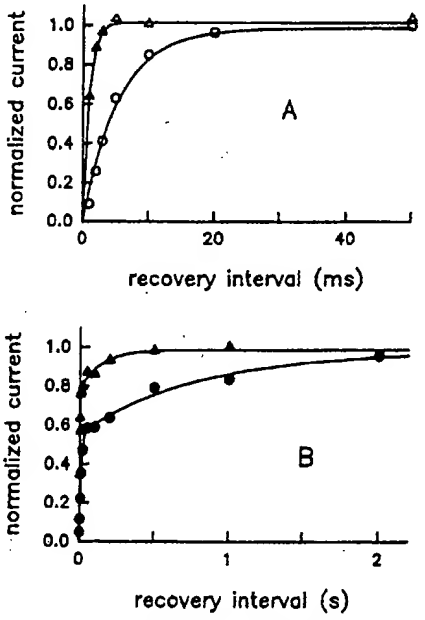

Fig. 13. Voltage dependence of Na^+ channel recovery. The rate of recovery from inactivation was assessed by the two-pulse protocol described in Fig. 10, but with the membrane potentials during the recovery intervals set to −85 mV (*circles*) and −128 mV (*triangles*), in control conditions (A) and in the presence of 50 μM lidocaine (B). The *smooth lines* were according to the equations given in Fig. 10, with the following time constants: A, τ = 5.5 and 1.0 msec for recovery pulses to −85 mV and −128 mV, respectively; B, τ_1 = 10.9 and 1.6 and τ_2 = 775 and 136 msec for −85 mV and −128 mV, respectively. Note the different time scales for A and B.

short to reach steady state conditions in the presence of the drugs, probably because of the relatively slow rate of drug dissociation during hyperpolarizing prepulses and slow association during depolarizing prepulses (see Figs. 9 and 11). Thus, a more accurate measure of steady state inactivation was obtained by varying the holding potential for 1 min before application of the test pulses. The dependence of steady state inactivation on prepulse duration could also be explained if the drugs stabilize Na^+ channels in "slow" inactivation states (30, 35, 36). These slow inactivation states have time constants of hundreds of milliseconds to many seconds and, therefore, would not be measured with short prepulses. Na^+ channels in CNaIIA-1 cells appear to have slow inactivation states, although they have not been studied in detail. The role, if any, of slow inactivation in the effects of anticonvulsants and local anesthetics in CNaIIA-1 cells is not clear and requires further investigation.

The drugs bound to both open and inactivated channels; however, association was faster to open channels. Similar fast association to open Na^+ channels has been observed for lidocaine in rabbit cardiac muscle (37) and toad sciatic nerve fibers (38). These results are consistent with the model proposed by Hille (19), in which local anesthetics bind rapidly to open channels by a hydrophilic route through the cytoplasm but bind more slowly to inactivated channels by a hydrophobic route through the plasma membrane.

The mechanism by which local anesthetic, antiarrhythmic, and anticonvulsant drugs slow channel repriming is not well understood. Slow repriming could reflect either slow drug dissociation from inactivated or resting channels or slow conversion of drug-bound channels from the inactivated to the resting states. Drug-bound Na^+ channels in CNaIIA-1 cells recovered more rapidly at hyperpolarized membrane potentials. Similar voltage dependence has been observed for lidocaine in cardiac cells (12, 37) and phenytoin in mouse neuroblastoma cells (30). Thus, in these preparations, there is a voltage-dependent, rate-limiting step for repriming of drug-bound channels. However, no voltage dependence of repriming was reported for lidocaine in toad sciatic nerve (38) or squid axon (39). This suggests that there may be different mechanisms of drug action for different types of Na^+ channels or that different recovery steps may be rate limiting.

Verapamil as a Na^+ channel blocker. Verapamil was a surprisingly potent blocker of rat brain Na^+ channels in CNaIIA-1 cells. The concentrations of verapamil used in this study were more than 10 times higher than those that are effective in blocking cardiac Ca^{2+} channels (40, 41). However, because both the tonic and use-dependent effects of verapamil were quite pronounced, it will be interesting to determine whether it also blocks cardiac Na^+ channels at concentrations closer to those at which it is an effective Ca^{2+} antagonist. An important implication of the results is that, when both Na^+ and Ca^{2+} channels are present, effects that are attributed strictly to verapamil block of Ca^{2+} channels may also be due, at least in part, to block of Na^+ channels.

It has previously been shown that, at concentrations ranging from 50 to 200 μM, verapamil and its methoxy derivative D600 block Na^+ currents in squid axons and cardiac muscle cells (14, 42) and inhibit veratridine-activated Na^+ flux in rat synaptosomes, chick cardiac cells, and mouse neuroblastoma cells (43, 44). However, the electrophysiological properties of this block were not well characterized in any of these studies. In this

study, we found that verapamil produced strong negative shifts in steady state inactivation and pronounced use-dependent block. These characteristics were similar to the effects of local anesthetics and anticonvulsants, suggesting that these drugs all have a similar mode of action. However, in several respects, the properties of verapamil block differed from those of the other drugs. For example, compared with phenytoin, carbamazepine, or lidocaine, verapamil bound more rapidly to open channels and more slowly to inactivated channels. Repriming of verapamil-bound channels was also quite slow, compared with the other drugs. In these respects, the characteristics of verapamil block of Na^+ channels were more similar to its effects on Ca^{2+} channels (40). This suggests that verapamil may have a similar mechanism of action for these two channel types and may act at analogous receptor sites on both.

Acknowledgment

We thank C. Warner for preparation of cell cultures.

References

1. Hille, B. *Ionic Channels of Excitable Membranes*. Sinauer Associates, Inc., Sunderland, MA (1984).
2. Agnew, W. S. Voltage-regulated sodium channel molecules. *Annu. Rev. Physiol.* **46**:517–530 (1984).
3. Catterall, W. A. Molecular properties of voltage-sensitive sodium channels. *Annu. Rev. Biochem.* **55**:953–985 (1986).
4. Barchi, R. L. Probing the molecular structure of the voltage-dependent sodium channel. *Annu. Rev. Neurosci.* **11**:455–495 (1988).
5. Catterall, W. A. Structure and function of voltage-sensitive ion channels. *Science (Washington D. C.)* **242**:50–61 (1988).
6. Rogart, R. B., L. L. Cribbs, L. K. Muglia, and D. D. Kephart. Molecular cloning of a putative tetrodotoxin-resistant rat heart Na^+ channel isoform. *Proc. Natl. Acad. Sci. USA* **86**:8170–8174 (1990).
7. Trimmer, J. S., S. S. Cooperman, S. A. Tomiko, J. Y. Zhou, S. M. Crean, M. B. Boyle, R. G. Kallen, Z. H. Sheng, R. L. Barchi, F. J. Sigworth, R. H. Goodman, W. S. Agnew, and G. Mandel. Primary structure and functional expression of a mammalian skeletal muscle sodium channel. *Neuron* **3**:33–49 (1989).
8. Numa, S. A molecular view of neurotransmitter receptors and ionic channels. *Harvey Lect.* **83**:121–165 (1989).
9. Auld, V. J., A. L. Goldin, D. S. Krafte, J. Marshall, J. M. Dunn, W. A. Catterall, H. A. Lester, N. Davidson, and R. J. Dunn. A rat brain Na^+ channel *alpha* subunit with novel gating properties. *Neuron* **1**:449–461 (1988).
10. Catterall, W. A. Common modes of drug action on Na^+ channels: local anesthetics, antiarrhythmics and anticonvulsants. *Trends Pharmacol. Sci.* **8**:57–65 (1987).
11. Rogawski, M. A., and R. J. Porter. Antiepileptic drugs: pharmacological mechanisms and clinical efficacy with consideration of promising developmental stage compounds. *Pharmacol. Rev.* **42**:223–286 (1990).
12. Hondeghem, L. M., and B. G. Katzung. Antiarrhythmic agents: the modulated receptor mechanism of action of sodium and calcium channel blocking drugs. *Annu. Rev. Pharmacol. Toxicol.* **24**:387–423 (1984).
13. Butterworth, J. F., IV, and G. R. Strichartz. Molecular mechanisms of local anesthesia: a review. *Anesthesiology* **72**:711–734 (1990).
14. Pidoplichko, V. I., and A. N. Verkhratskii. Frequency related blocking of sodium channels in the membrane of isolated rat cardiomyocytes by the calcium antagonist verapamil. *Fiziol. Zh. (Kiev)* **35**:87–89 (1989).
15. Walden, J., E.-J. Speckmann, and O. W. Witte. Suppression of focal epileptiform discharges by intraventricular perfusion of a calcium antagonist. *Electroencephalogr. Clin. Neurophysiol.* **61**:299–309 (1985).
16. Sokic, D. V., and M. S. Kovacevic. Treatment of status epilepticus with intravenous lidocaine. *Srp. Arkh. Tselok. Lek.* **117**:531–538 (1989).
17. Bingmann, D., E.-J. Speckmann, R. E. Baker, J. Ruijter, and B. M. de Jong. Differential antiepileptic effects of the organic calcium antagonists verapamil and flunarizine in neurons of organotypic neocortical explants from newborn rats. *Exp. Brain Res.* **72**:439–442 (1988).
18. Aicardi, G., and P. A. Schwartzkroin. Suppression of epileptiform burst discharges in CA3 neurons of rat hippocampal slices by the organic calcium channel blocker, verapamil. *Exp. Brain Res.* **81**:288–296 (1990).
19. Hille, B. Local anesthetics: hydrophilic and hydrophobic pathways for the drug-receptor reaction. *J. Gen. Physiol.* **69**:497–515 (1977).
20. Gordon, D., D. Merrick, V. Auld, R. Dunn, A. L. Goldin, N. Davidson, and W. A. Catterall. Tissue-specific expression of the RI and RII sodium channel subtypes. *Proc. Natl. Acad. Sci. USA* **84**:8682–8686 (1987).
21. Beckh, S., M. Noda, H. Lubbert, and S. Numa. Differential regulation of three sodium channel messenger RNAs in the rat central nervous system during development. *EMBO J.* **8**:3611–3616 (1989).
22. Westenbroek, R. E., D. K. Merrick, and W. A. Catterall. Differential subcellular localization of the R_I and R_{II} Na^+ channel subtypes in central neurons. *Neuron* **3**:695–704 (1989).
23. Scheuer, T., V. J. Auld, S. Boyd, J. Offord, R. Dunn, and W. A. Catterall. Functional properties of rat brain sodium channels expressed in a somatic cell line. *Science (Washington D. C.)* **247**:854–858 (1990).
24. Scheuer, T., J. W. West, L. Maechler, and W. A. Catterall. Efficient expression of rat brain sodium channel type IIA α subunits in Chinese hamster ovary cells. *Neuron*, in press.
25. Auld, V. J., A. L. Goldin, D. S. Krafte, W. A. Catterall, H. A. Lester, N. Davidson, and R. J. Dunn. A neutral amino acid change in segment IIS4 dramatically alters the gating properties of the voltage-dependent sodium channel. *Proc. Natl. Acad. Sci. USA* **87**:323–327 (1990).
26. Hamill, O. P., A. Marty, E. Neher, B. Sakmann, and F. J. Sigworth. Improved patch-clamp techniques for high-resolution current recording from cells and cell-free membrane patches. *Pflugers Arch.* **391**:85–100 (1981).
27. Marquardt, D. W. An algorithm for least squares estimation of nonlinear parameters. *J. Soc. Ind. Appl. Math.* **11**:431–441 (1963).
28. Bezanilla, F., and C. M. Armstrong. Inactivation of the sodium channel. I. Sodium current experiments. *J. Gen. Physiol.* **70**:549–566 (1977).
29. McLean, M. J., and R. L. Macdonald. Multiple actions of phenytoin on mouse spinal cord neurons in cell culture. *J. Pharmacol. Exp. Ther.* **227**:779–789 (1983).
30. Matsuki, N., F. N. Quandt, R. E. Ten Eick, and J. Z. Yeh. Characterization of the block of sodium channels by phenytoin in mouse neuroblastoma cells. *J. Pharmacol. Exp. Ther.* **228**:523–530 (1984).
31. Wakamori, M., M. Kaneda, Y. Oyama, and N. Akaike. Effects of chlordiazepoxide, chlorpromazine, diazepam, diphenylhydantoin, flunitrazepam and haloperidol on the voltage-dependent sodium current of isolated mammalian brain neurons. *Brain Res.* **494**:374–378 (1989).
32. Willow, M., and W. A. Catterall. Inhibition of binding of [^{3}H]batrachotoxinin A 20-*alpha*-benzoate to sodium channels by the anticonvulsant drugs diphenylhydantoin and carbamazepine. *Mol. Pharmacol.* **22**:627–635 (1982).
33. Willow, M., E. A. Kuenzel, and W. A. Catterall. Inhibition of voltage-sensitive sodium channels in neuroblastoma cells and synaptosomes by the anticonvulsant drugs diphenylhydantoin and carbamazepine. *Mol. Pharmacol.* **25**:228–234 (1984).
34. Willow, M., T. Gonoi, and W. A. Catterall. Voltage clamp analysis of the inhibitory actions of diphenylhydantoin and carbamazepine on voltage-sensitive sodium channels in neuroblastoma cells. *Mol. Pharmacol.* **27**:549–558 (1985).
35. Quandt, F. N. Modification of slow inactivation of single sodium channels by phenytoin in neuroblastoma cells. *J. Pharmacol. Exp. Ther.* **34**:557–565 (1988).
36. Khodorov, B., L. Shishkova, E. Peganov, and S. Revenko. Inhibition of sodium currents in frog Ranvier node treated with local anesthetics: role of slow sodium inactivation. *Biochim. Biophys. Acta* **433**:409–435 (1976).
37. Bean, B. P., C. J. Cohen, and R. W. Tsien. Lidocaine block of cardiac sodium channels. *J. Gen. Physiol.* **81**:613–642 (1983).
38. Chernoff, D. M. Kinetic analysis of phasic inhibition of neuronal sodium currents by lidocaine and bupivacaine. *Biophys. J.* **58**:53–68 (1990).
39. Yeh, J. Z., and J. Tanguy. Na channel activation gate modulates slow recovery from use-dependent block by local anesthetics in squid giant axons. *Biophys. J.* **47**:685–694 (1985).
40. Lee, K. S., and R. W. Tsien. Mechanism of calcium channel blockade by verapamil, D600, diltiazem and nitrendipine in single dialysed heart cells. *Nature (Lond.)* **302**:790–794 (1983).
41. Kanaya, S., P. Arlock, B. G. Katzung, and L. M. Hondeghem. Diltiazem and verapamil preferentially block inactivated cardiac calcium channels. *J. Mol. Cell. Cardiol.* **15**:149–150 (1983).
42. Baker, P. F., H. Meves, and E. B. Ridgway. Effects of manganese and other agents on the calcium uptake that follows depolarization of squid axons. *J. Physiol. (Lond.)* **321**:511–526 (1973).
43. Galper, J., and W. A. Catterall. Inhibition of sodium channels by D600. *Mol. Pharmacol.* **15**:174–178 (1979).
44. Nachsen, D. A., and M. P. Blaustein. The effects of some organic "calcium antagonists" on calcium flux in presynaptic nerve terminals. *Mol. Pharmacol.* **16**:579–586 (1979).

Send reprint requests to: Dr. William A. Catterall, Department of Pharmacology, SJ-30, University of Washington, School of Medicine, Seattle, WA 98195.

Molecular Pharmacology Volume 40, Number 5, November 1991

CONTENTS

ACCELERATED COMMUNICATIONS

ARTICLES

Continued

MOLECULAR PHARMACOLOGY (ISSN 0026-895x) is an official publication of The American Society for Pharmacology and Experimental Therapeutics and is published monthly, two volumes a year, beginning in January and July, by Williams & Wilkins, 428 East Preston Street, Baltimore, MD 21202-3993. Price per year: USA individual rate $100; all other countries, surface mail $130. USA institutional rate $210, all other countries, surface mail $240. Single copies $18 ($21 foreign). (Prices subject to change.) Indexed by *Index Medicus, Current Contents/Life Sciences, Excerpta Medica,* and *Current Awareness in Biological Sciences.* All subscription orders should be addressed to Molecular Pharmacology, 428 East Preston Street, Baltimore, MD 21202-3993.

Second Class Postage paid at Baltimore, MD, and at additional mailing offices. The GST Tax number for Canadian subscribers is 123394371. POSTMASTER: Send address changes to MOLECULAR PHARMACOLOGY, 428 East Preston Street, Baltimore, MD 21202-3993.

MOLECULAR PHARMACOLOGY

AN INTERNATIONAL JOURNAL

VOLUME 40
NUMBER 5
NOVEMBER 1991

FOUNDED BY AVRAM GOLDSTEIN–1965

ASPET

A PUBLICATION OF THE AMERICAN SOCIETY FOR PHARMACOLOGY AND EXPERIMENTAL THERAPEU

3. E. H. Buhl, K. Halasy, P. Somogyi, *Nature* **368**, 823 (1994).
4. X.-G. Li, P. Somogyi, J. M. Tepper, G. Buzsáki, *Exp. Brain Res.* **90**, 519 (1992); X.-G. Li, P. Somogyi, A. Ylinen, G. Buzsáki, *J. Comp. Neurol.* **339**, 181 (1994).
5. D. D. Kunkel, J.-C. Lacaille, P. A. Schwartzkroin, *Synapse* **2**, 382 (1988); P. S. Buckmaster, B. W. Strowbridge, D. D. Kunkel, D. L. Schmiege, P. A. Schwartzkroin, *Hippocampus* **2**, 349 (1992); Z.-S. Han, E. H. Buhl, Z. Lorinczi, P. Somogyi, *Eur. J. Neurosci.* **5**, 395 (1993); K. Halasy and P. Somogyi, *ibid.*, p. 411; A. Gulyas *et al.*, *Nature* **366**, 683 (1993); A. Gulyas, R. Miles, N. Hajos, T. F. Freund, *Eur. J. Neurosci.* **5**, 1729 (1993); N. Tamamaki, K. Abe, Y. Nojyo, *Brain Res.* **452**, 255 (1988); N. Tamamaki and Y. Nojyo, *J. Comp. Neurol.* **291**, 509 (1990); *ibid.* **303**, 435 (1991).
6. A. Sik, M. Tamamaki, T. F. Freund, *Eur. J. Neurosci.* **5**, 1719 (1993).
7. D. G. Amaral and M. Witter, *Neuroscience* **31**, 571 (1989); F. H. Lopes da Silva, M. Witter, P. H. Boeijinga, A. Lohman, *Physiol. Rev.* **70**, 453 (1990).
8. S. R. Vincent and H. Kimura, *Neuroscience* **46**, 755 (1992).
9. The fimbria-fornix, the cingulate bundle, the supracallosal stria and part of the corpus callosum, and the cingulate cortex were removed by aspiration, leaving the dorsal hippocampus completely denervated from its subcortical inputs [G. Buzsáki, F. H. Gage, J. Czopf, A. Björklund, *Brain Res.* **400**, 334 (1987)].
10. H. H. Young, J. B. Furness, A. W. R. Shuttleworth, D. S. Bredt, S. H. Snyder, *Histochemistry* **97**, 375 (1992); J. G. Valtschanoff, R. J. Weinberg, V. N. Kharazia, M. Nakane, H. H. H. W. Schmidt, *J. Comp. Neurol.* **331**, 111 (1993).
11. Biocytin (3%) was injected extracellularly in the CA1 stratum oriens with micropipettes (resistance, 1 to 2 megohms) by 2.0-μA depolarizing current pulses for 15 min in 20 urethane-anesthetized rats. Nine of the rats underwent fimbria-fornix lesion 7 to 20 days before the injection (*9*).
12. Rats were anesthetized with urethane. Stimulating electrodes were inserted into the ventral hippocampal commissure. Intracellular recording was carried out with glass micropipettes filled with biocytin solution (3% in 1 M potassium acetate; resistance, 60 to 95 megohms). After the physiological properties of the cell were determined, biocytin was injected with depolarizing current pulses (1 to 5 nA) for 5 to 60 min. After 2 to 16 hours, rats were perfused with a fixative (*4*). The avidin-biotinylated horseradish peroxidase complex reaction was used to visualize the biocytin-filled cells [K. Horikawa and W. Armstrong, *J. Neurosci. Methods* **25**, 1 (1988)]. Axon collaterals were drawn with the aid of a drawing tube (*4*, *6*).
13. J. C. Lacaille, A. Mueller, D. D. Kunkel, P. A. Schwartzkroin, *J. Neurosci.* **7**, 1979 (1987); Y. Kawaguchi, H. Katsumaru, T. Kosaka, C. W. Heizmann, K. Hama, *Brain Res.* **416**, 369 (1987).
14. The sections were treated with 1% OsO_4 for 1 hour, dehydrated, counterstained with uranyl-acetate, and finally embedded in Durcupan (Fluka, Basel, Switzerland). Selected areas were re-embedded for ultrathin sectioning. Serial ultrathin sections were cut and mounted on single-slot Formvar-coated grids and counterstained with lead acetate (*6*).
15. G. Buzsáki, *Neuroscience* **31**, 551 (1989); T. H. Bullock, G. Buzsáki, M. C. McClune, *ibid.* **38**, 609 (1990); G. Buzsáki, Z. Horváth, R. Urioste, J. Hetke, K. Wise, *Science* **256**, 1025 (1992); A. Ylinen, A. Sik, A. Bragin, G. Jando, G. Buzsáki, *J. Neurosci.*, in press.
16. J. Holsheimer and F. H. Lopes da Silva, *Exp. Brain Res.* **77**, 69 (1989); G. Buzsáki, M. Hsu, C. Slamka, F. H. Gage, Z. Horváth, *Hippocampus* **1**, 163 (1991).
17. R. J. Douglas and K. A. C. Martin, *Neural Comp.* **2**, 283 (1990); W. W. Lytton and T. J. Sejnowski, *J. Neurophysiol.* **66**, 1059 (1991).
18. T. J. O'Dell, R. S. Hawkins, E. R. Kandel, O. Arancio, *Proc. Natl. Acad. Sci. U.S.A.* **88**, 11285 (1991); E. M. Schuman and D. V. Madison, *Science* **254**, 1503 (1991); D. S. Bredt and S. H. Snyder, *Neuron* **8**, 3 (1992); S. A. Small, E. R. Kandel, R. D. Hawkins, *Science* **260**, 1946 (1993); E. M. Schuman and D. V. Madison, *ibid.* **263**, 532 (1994).
20. R. S. Sloviter and G. Nilaver, *J. Comp. Neurol.* **256**, 42 (1987).
21. R. A. Nicoll, R. C. Malenka, J. A. Kauer, *Physiol. Rev.* **79**, 513 (1990).
22. Supported by NIH, the Human Frontier Science Program, the Whitehall Foundation, and the Finnish and the Hungarian academies of sciences (F5531). We thank D. G. Amaral, P. Andersen, T. V. P. Bliss, T. F. Freund, M. Hsu, E. R. Kandel, P. A. Schwartzkroin, J. M. Tepper, and R. Traub for helpful suggestions.

29 December 1993; accepted 10 August 1994

Molecular Determinants of State-Dependent Block of Na^+ Channels by Local Anesthetics

David S. Ragsdale, Jancy C. McPhee, Todd Scheuer, William A. Catterall

Sodium ion (Na^+) channels, which initiate the action potential in electrically excitable cells, are the molecular targets of local anesthetic drugs. Site-directed mutations in transmembrane segment S6 of domain IV of the Na^+ channel α subunit from rat brain selectively modified drug binding to resting or to open and inactivated channels when expressed in *Xenopus* oocytes. Mutation F1764A, near the middle of this segment, decreased the affinity of open and inactivated channels to 1 percent of the wild-type value, resulting in almost complete abolition of both the use-dependence and voltage-dependence of drug block, whereas mutation N1769A increased the affinity of the resting channel 15-fold. Mutation I1760A created an access pathway for drug molecules to reach the receptor site from the extracellular side. The results define the location of the local anesthetic receptor site in the pore of the Na^+ channel and identify molecular determinants of the state-dependent binding of local anesthetics.

Voltage-gated Na^+ channels are integral membrane proteins that are responsible for the initial, rapid depolarization of the action potential in nerve and muscle cells. At negative membrane potentials, most Na^+ channels are in closed, resting states. In response to membrane depolarization, the channels open in a few hundred microseconds, resulting in Na^+ influx through a Na^+-selective pore, and then convert to a nonconducting inactivated state. The rat brain Na^+ channel consists of α (260 kD), β1 (36 kD), and β2 (33 kD) subunits (*1*). The α subunit is composed of four homologous domains (I through IV), each with six α-helical transmembrane segments (S1 through S6) (*2*, *3*). The α subunit forms functional channels when expressed in mammalian cells (*4*, *5*) or *Xenopus* oocytes (*6*), although coexpression of β1 is required for normal kinetic properties in oocytes (*7*).

Local anesthetics block Na^+ channels with complex voltage- and frequency-dependent properties that are important for the clinical efficacy of the drugs and that indicate that drug binding is modulated by channel state (*8*–*11*). The state-dependence of block can be explained by an allosteric model in which a modulated drug receptor has a higher affinity when channels are open or inactivated than when the channels are resting (*8*–*10*). Biophysical evidence is consistent with the hypothesis that this receptor site is on the α subunit in the ion-conducting pore and accessible from the cytoplasmic side of the channel (*9*, *12*–*15*). Determination of the amino acids that form the local anesthetic receptor site is important for understanding the complex action of these drugs. The S6 segment in domain IV (segment IVS6) of Ca^{2+} channels and the S6 segment of K^+ channels have been implicated in the binding of pore blockers (*16*). We used site-directed mutagenesis to examine the function of segment IVS6 of the α subunit of the Na^+ channel in local anesthetic action. Mutations in IVS6 altered the sensitivity of Na^+ channels to local anesthetics, indicating that amino acids in this region are determinants of the action of these drugs.

Rat brain type IIA Na^+ channels (*3*) expressed in *Xenopus* oocytes (wild type) (*17*, *18*) were blocked ~40% by 200 μM etidocaine, a tertiary amine local anesthetic, when the oocytes were stimulated infrequently (1 pulse per 20 s) (Fig. 1A). This tonic block mainly reflects drug binding to resting channels, the channel state that predominated at the holding potential of −90 mV (*8*–*10*). To determine whether amino acids in IVS6 are involved in local anesthetic action, we substituted alanine sequentially for the native amino acids at each position from F1756 to L1776 (Fig. 1A) (*18*). Alanine was chosen because it changes the size and chemical properties of the residues but has minimal effects on protein secondary structure (*19*).

Most IVS6 mutants exhibited a 40 to 50%

Department of Pharmacology, University of Washington, Seattle, WA 98195, USA.

tonic block by 200 μM etidocaine at a holding potential of −90 mV like wild type (Fig. 1A). However, mutants I1761A, F1764A, V1766A, V1767A, and N1769A displayed significantly altered sensitivity (Fig. 1A). N1769A was almost completely blocked by 200 μM etidocaine, whereas I1761A, V1766A, and V1767A were ~70 to 75% blocked. In contrast, F1764A was only inhibited 20%. The results suggest that the amino acids at these positions are determinants of local anesthetic binding to resting Na^+ channels. However, because of the state-dependent modulation of drug binding, it was also possible that these effects were secondary to changes in the voltage dependence of inactivation rather than a reflection of actual changes in resting channel affinity. Therefore, to determine the mechanisms underlying the effects of these mutations, we examined the voltage dependence of tonic block over a broad range of holding potentials.

For the wild-type channel, in the absence of etidocaine, the relation between current amplitude and holding potential formed a characteristic inactivation curve with a midpoint ($V_{1/2}$) of about −54 mV (Fig. 1B). Etidocaine (200 μM) reduced currents through wild-type channels at all voltages (Fig. 1B). Block was enhanced at depolarized holding potentials because of a greater availability of inactivated channels and was relieved at hyperpolarized holding potentials. At potentials more negative than −100 mV, the block approached a plateau of approximately 35% that was independent of holding potential. This indicates that inactivation was completely relieved at these potentials, so inhibition reflected only drug binding to resting Na^+ channels. The dependence of this resting block on etidocaine concentration was described by a 1:1 binding relation with a resting channel equilibrium dissociation constant (K_r) of 325 μM (Fig. 1D).

The control inactivation curve for V1766A was almost identical to that of wild-type channels (Fig. 1B). However, mutations I1761A, V1767A, and N1769A shifted $V_{1/2}$ negatively by 7 to 13 mV (Fig. 1B), whereas mutation F1764A shifted $V_{1/2}$ 8 mV positively (Fig. 1B). The negative shifts in $V_{1/2}$ for I1761A, V1767A, and N1769A increased the proportion of inactivated channels at moderate holding potentials, which could have caused part of the increased tonic block with these mutants. This was probably the main effect of V1767A because most of the increased block observed at −90 mV was relieved by strong hyperpolarization, and resting block was similar to wild type at −140 mV (Fig. 1B).

In contrast, resting block at the most negative membrane potentials for I1761A, V1766A, and N1769A was significantly greater than that of wild-type channels, indicating that these mutations altered the sensitivity of resting channels to etidocaine (Fig. 1, B through D). For I1761A and V1766A, resting block with 200 μM etidocaine was 55 to 60% (Fig. 1B), and K_r was ~100 μM (Fig. 1D). Mutant N1769A was almost completely blocked by 200 μM etidocaine at all potentials (Fig. 1B), and there was no detectable relief from block even when oocytes were held at −140 mV for up to 1 min. At a concentration of 10 μM etidocaine, block reached a plateau of about 40% at hyperpolarized potentials (Fig. 1C), indicating that the inhibition of Na^+ currents was due to an increased sensitivity of resting channels. K_r was 20 μM, a 15-fold increase in sensitivity as compared with wild-type channels (Fig. 1D).

In contrast to the mutations described above, F1764A caused a significant decrease in resting block. With 200 μM etidocaine, resting block was only 15% (Fig. 1B), and K_r was 1 mM, threefold greater than for wild-type channels (Fig. 1D).

The voltage dependence of tonic block resulted in a concentration-dependent negative shift ($\Delta V_{1/2}$) in the midpoint of inac-

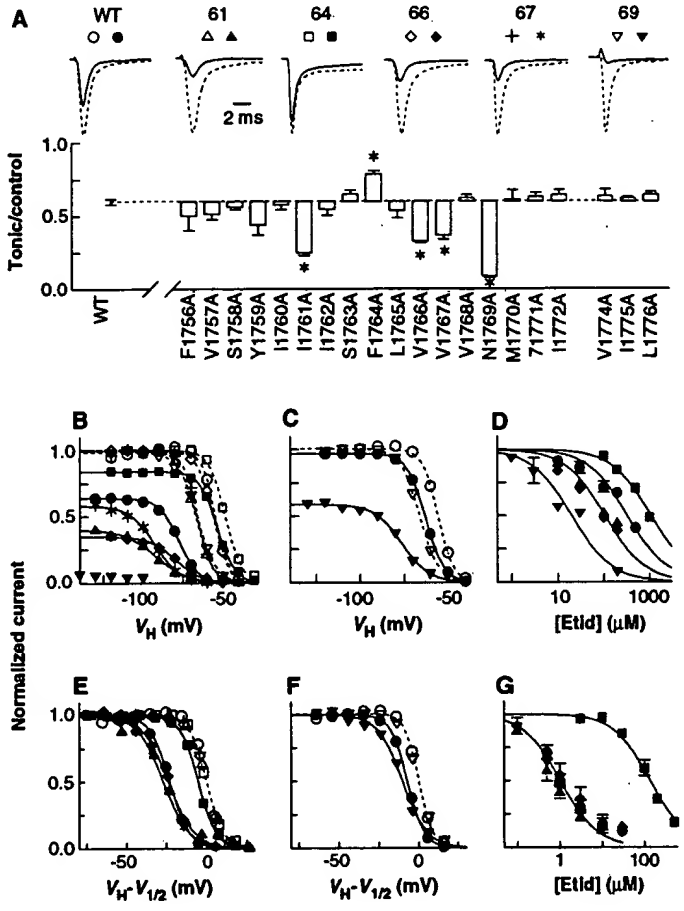

Fig. 1. Mutations in IVS6 alter tonic block by etidocaine. (**A**) Typical current records for wild-type (WT) and selected mutants in control (dashed lines) and 200 μM etidocaine (solid lines) experiments are shown above the histogram. Unless indicated, all currents were elicited by 15-ms pulses to 0 mV. The histogram shows mean amplitudes of currents ± SEM (n = 3 to 28) for wild-type and mutant channels after block by 200 μM etidocaine. The data were normalized with respect to control currents elicited before drug application and plotted as deviations from the wild-type mean (dashed line). The asterisks show means that were significantly different from wild type [Student's t test; $P < 0.05$]. For N1769A, activation was shifted positively by 20 mV, so currents were evoked by pulses to +20 mV. (**B** and **C**) We assessed the voltage dependence of tonic block by test pulses applied after stepping to various holding potentials for 10 s. Peak currents were plotted as a function of holding potential (V_H). Each set of symbols represents data from a representative oocyte in control conditions and after application of 200 (B) or 10 (C) μM etidocaine for wild type (control, ○; with etidocaine, ●), I1761A (△, ▲), F1764A (□, ■), V1766A (◇, ◆), V1767A (+, *), and N1769A (▽, ▼). Data for each experiment were normalized with respect to the largest control currents. The theoretical curves through control (dashed lines) and etidocaine (solid lines) data are least-squares fits of $a/[1 + \exp(V_H - V_{1/2})/k]$, where a is a scaling factor, $V_{1/2}$ is the midpoint of the curve, and k is a slope factor. (**D**) Resting block as indicated by values for a determined from fits of the equation in (B) and (C) were plotted as a function of etidocaine concentration [Etid] for wild type (●), I1761A (▲), F1764A (■), V1766A (◆), and N1769A (▼). The theoretical curves are according to $(1/(1 + [\text{etid}]/K_r))$, where K_r is the midpoint of the dose-effect curve. (**E** and **F**) We replotted data in (B) (200 μM etidocaine) and in (C) (10 μM etidocaine) to demonstrate the shifts in $V_{1/2}$ caused by the drug. We normalized the data and theoretical curves in control and etidocaine conditions to the same maximum value and shifted them on the voltage axis until the control curves superimposed with $V_{1/2}$ = 0 mV. (**G**) We determined block of inactivated channels for wild type (●), I1761A (▲), F1764A (■), V1766A (◆), and N1769A (▼) by stepping to −40 mV for 10 s and then giving a 10-ms recovery pulse to −110 mV, followed by a test pulse to 0 mV. The peak current evoked by the test pulse was normalized to control and plotted as a function of etidocaine concentration. The smooth line is according to $1 - (1/(1 + [\text{etid}]/K_i))$.

tivation. This shift is a consequence of enhanced drug binding to inactivated channels (9, 10). To directly compare $\Delta V_{1/2}$ for wild type and mutants, we shifted curves in Fig. 1, B and C, obtained in the absence and in the presence of etidocaine along the voltage axis until the control curves superimposed, and the currents in the presence of drug were scaled to the same maximum value as that of the control (Fig. 1, E and F). For wild type, $\Delta V_{1/2}$ was about −7 mV in the presence of 10 μM etidocaine (Fig. 1F) and −24 mV with 200 μM etidocaine (Fig. 1E). The $\Delta V_{1/2}$'s for I1761A, V1766A (Fig. 1E), and N1769A (Fig. 1F) were approximately equal to those for wild type, indicating similarly strong drug binding to inactivated channels. In contrast, F1764A reduced $\Delta V_{1/2}$ to −7 mV (Fig. 1E), suggesting a decrease in the affinity of the inactivated channel.

To examine drug binding to inactivated Na^+ channels directly (Fig. 1G), we first stepped the holding potential from −90 mV to −40 mV for 10 s, which inactivated most Na^+ channels but caused little channel activation. The long pulse duration ensured that drug binding to inactivated channels reached steady state. The membrane potential was then stepped to −110 mV for 10 ms, which allowed recovery of unblocked, fast-inactivated channels but which was short enough to prevent drug dissociation from most blocked channels. The availability of unblocked, resting channels was then assessed by a test pulse to 0 mV. In control conditions, this protocol caused a 40% reduction in current amplitude due to slow inactivation during the long conditioning prepulse, from which channels did not recover during the 10-ms repolarization (20). In the presence of the drug, there was an additional decrease in current amplitude due to drug binding to inactivated channels during the conditioning pulse. For wild type, this drug-dependent decrease in current was described by a 1:1 binding relation with a dissociation constant for inactivated channels (K_i) of 1 μM (Fig. 1G), 1/300 of the value of K_r for binding to the resting state. The K_i's for I1761A, V1766A, and N1769A were virtually identical to that for wild type (Fig. 1G). Thus, mutations that caused 3- to 15-fold increases in the affinity for the resting state had no detectable effect on K_i for binding to the inactivated state. In contrast, K_i for F1764A was 130 μM (Fig. 1G). Apparently the properties of the residue at this site are a determinant of tonic block due to drug binding to inactivated Na^+ channels.

Use-dependent block of Na^+ channels by local anesthetics during rapid trains of stimulus pulses results from binding of the drug to open and inactivated channels during depolarizing pulses and from slowed recovery of drug-bound channels between pulses. We assessed use-dependent block by applying 15-ms pulses to 0 mV at a frequency of 2 Hz in the presence of 200 μM etidocaine. For wild-type channels, this resulted in a further 60% use-dependent block of the Na^+ current that remained after the steady state for tonic block was reached (Fig. 2A, wild type). A number of mutations in IVS6 decreased use-dependent block in comparison to wild type. The largest decreases in use-dependent block were seen for the mutants I1760A, F1764A, and Y1771A (Fig. 2A).

Use-dependent block of wild-type channels was just detectable when pulses were applied at 0.2 Hz, was half maximal at 1 to 2 Hz, and approached 100% at 20 Hz (Fig. 2B). Mutants I1760A, F1764A, and Y1771A exhibited less use-dependent block over this whole range of stimulus frequencies; however, the different mutants showed different frequency-dependence profiles. Use-dependent block in I1760A was dependent on frequency like wild type but was shifted to five times higher frequencies (Fig. 2B), whereas block in Y1771A was less frequency-dependent (Fig. 2B), and F1764A was virtually insensitive to use-dependent block up to 20 Hz (Fig. 2B). These different profiles suggested that the mutations altered use-dependent block through different mechanisms.

In principle, mutations could alter use-dependent block during a pulse train either by altering the amount of drug that binds to open and inactivated channels during the depolarizing pulses or by altering the rate at which the drug dissociates between the pulses as the channels convert back to the resting state. We examined these parameters for wild-type, I1760A, F1764A, and Y1771A channels by determining the fraction of channels blocked during 15-ms conditioning pulses to 0 mV and the time course of recovery of these blocked channels after the holding potential was returned to −90 mV. Recovery in control conditions simply reflected the rate of recovery from fast inactivation, which was monoexponential, with a time constant of 2 to 6 ms at −90 mV (15). In the presence of 200 μM etidocaine, recovery had two kinetic components, one reflecting the fast recovery from inactivation of channels that were not blocked during the conditioning

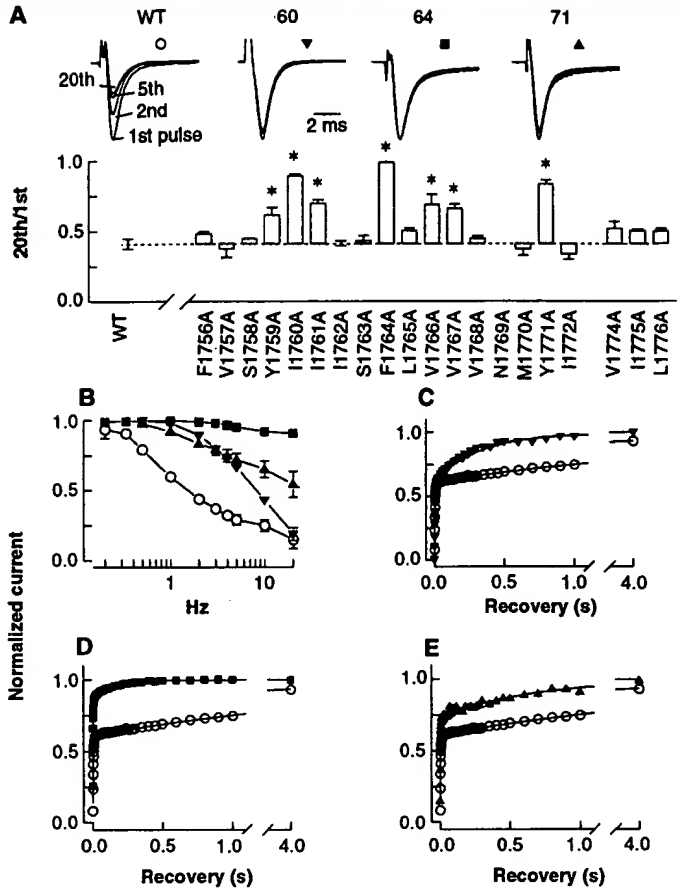

Fig. 2. IVS6 mutations alter use-dependent block by etidocaine. (**A**) The histogram shows the ratios (mean ± SEM; n = 2 to 22; *, $P < 0.05$) of the peak currents evoked by the 20th and 1st pulses in a 2-Hz pulse train in the presence of 200 μM etidocaine for wild-type (WT) and mutant channels. The traces above the graph are typical records showing currents elicited by the 1st, 2nd, 5th, and 20th pulses for the wild-type and selected mutants. (**B**) We assessed the dependence of use-dependent block on stimulus frequency for wild type (○), I1760A (▼), F1764A (■), or Y1771A (▲) channels by applying pulse trains of varying frequencies in the presence of 200 μM etidocaine. The mean ratios of the 20th/1st pulses were plotted as a function of stimulus frequency. (**C** through **E**) We examined channel recovery after depolarization-induced block by 200 μM etidocaine by giving a 15-ms conditioning pulse to 0 mV, followed by a recovery interval of varying duration at −90 mV and a test pulse to 0 mV. Peak test pulse current/peak conditioning pulse current was plotted as a function of the recovery interval. The graphs show typical experiments for I1760A (C, ▼), F1764A (D, ■), and Y1771A (E, ▲), in each case compared with the same wild-type experiment (○). The smooth lines are least-squares fits of the sum of two exponentials.

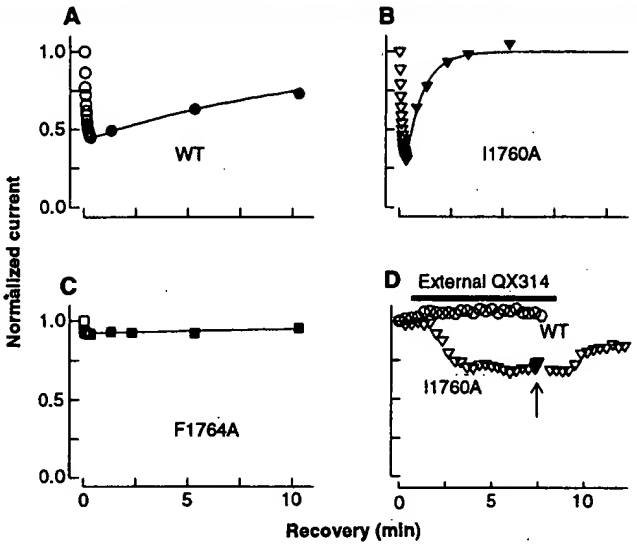

Fig. 3. Block of wild-type and mutant channels by QX314. We studied the action of internally applied QX314 by microinjecting 50 nl of a 4 mM solution of QX314 in oocytes expressing (**A**) wild-type, (**B**) I1760, and (**C**) F1764 channels. We assumed an average oocyte volume of 1 μl, so this resulted in an intracellular QX314 concentration of ~200 μM. The oocytes were then voltage-clamped at −90 mV, and 10 min after microinjection, a 1-Hz train of 15-ms-long pulses to 0 mV was applied, resulting in use-dependent block (open symbols). We then assessed the rate of repriming at −90 mV by giving infrequent stimulus pulses (filled symbols). Each panel shows peak currents from a single experiment, normalized with respect to the current elicited by the first pulse in the train. The smooth lines through the recovery data are exponential fits. (**D**) Action of externally applied QX314. QX314 (500 μM) was applied by superfusion to oocytes expressing wild-type (○) or I1760A (▽) channels for the time indicated by the bar. Currents were evoked by pulses applied at 20-s intervals. At the arrow, a 2-Hz pulse train was applied to the oocyte expressing I1760A channels. The data in each experiment were normalized with respect to the control currents.

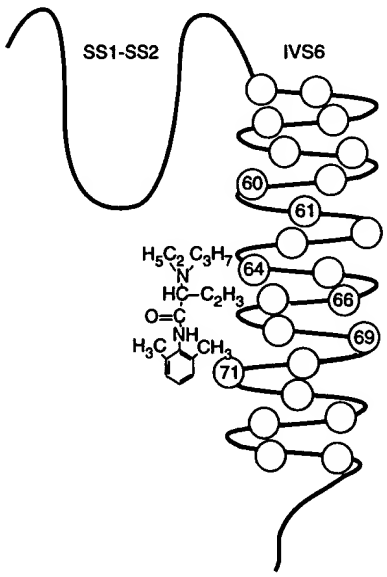

Fig. 4. Proposed orientation of amino acids in IVS6 with respect to a bound local anesthetic molecule in the ion-conducting pore. Segment SS1–SS2, which also contributes to the pore (*27*), is shown as well. Amino acids at positions 1760, 1764, and 1771 are shown facing the pore lumen.

pulse, and a second, slower component reflecting the slow dissociation of drug from channels that were blocked during the conditioning pulse. The time constant of the slow component of recovery gives a measure of the rate of drug dissociation from blocked channels at hyperpolarized potentials, whereas the proportion of slow recovery gives a measure of the fraction of channels that bound drug during the conditioning pulse.

About 40% of wild-type channels bound drug during the conditioning pulse, and these channels recovered with a time constant of 2.4 s (Fig. 2, C through E). For I1760A, the proportion of slowly recovering channels was almost identical to that for wild type (Fig. 2C), indicating that this mutation did not alter the affinity of the open or inactivated states for etidocaine. However, the recovery rate for drug-bound channels was eight times faster than for wild type. Thus, I1760A accelerated the escape of drug from closed channels at negative potentials, accounting for the altered frequency dependence of block.

In contrast to wild type and I1760A, only about 15% of the F1764A channels bound drug during the conditioning pulse, and the recovery of drug-bound channels was 20 times faster than for wild type (Fig. 2D). This indicates that the F1764A mutation reduced the affinity of open and fast inactivated channels for etidocaine, resulting in almost complete abolition of use-dependent block. This result is consistent with the high K_i value determined for F1764A (Fig. 1G). Y1771A also reduced drug binding during the conditioning pulse and speeded recovery of drug-bound channels (Fig. 2E), but the effect was less than for F1764A. Thus, Y1771A also reduced open or inactivated channel affinity but to a lesser extent. The K_i for Y1771A, determined by the conditioning pulse protocol in Fig. 1G, was 35 μM.

Quaternary amines like QX314 are local anesthetic derivatives that are permanently positively charged and are impermeant to cell membranes. They are ineffective when applied extracellularly but are potent use-dependent blockers when applied intracellularly (*12*, *13*). These drugs act mainly on open Na^+ channels through a cytoplasmic, hydrophilic pathway that is occluded by the activation and inactivation gates (*9*, *13*, *14*). Intracellularly applied QX314 was a use-dependent blocker of wild-type Na^+ channels during a 1-Hz stimulus train (Fig. 3A). The time constant for recovery from QX314 block at −90 mV was approximately 12 min (Fig. 3A), which was 1/300 of the rate of recovery from etidocaine block. This slow recovery was probably caused by trapping of the charged drug when the activation or inactivation gates closed (*13*, *21*, *22*). I1760A displayed similar sensitivity to use-dependent block by QX314 (Fig. 3B); however, the time constant for recovery was only 0.8 min (Fig. 3B). Thus, complete recovery of I1760A channels blocked by QX314 took only a few minutes, as compared with more than 30 min for wild-type channels. The wild-type and I1760A channels exhibited similar voltage dependence for activation, indicating that the fast recovery of I1760A was not due to greater frequency of channel openings during the recovery intervals (*21*, *22*). Apparently, the mutation created another pathway or lowered the energy barrier of an existing pathway for drug escape from closed channels.

Because I1760A is close to the extracellular side of IVS6, the mutation at this site might allow QX314 to escape from closed channels into the extracellular bath. If so, then this mutation would also create an access pathway for extracellular drug. To test this, we examined the action of extracellular QX314 on wild-type and I1760A channels. Bath-applied QX314 had no effect on wild-type channels (Fig. 3D) (*12*, *13*); however, it rapidly blocked I1760A channels (Fig. 3D). Thus, mutation I1760A created an access pathway between the drug binding site and the extracellular medium that is normally occluded for quaternary drugs. This pathway probably also explains the rapid recovery of I1760A channels blocked by tertiary drugs. A 2-Hz train of pulses (Fig. 3D, arrow) applied after the drug did not produce use-dependent block of I1760A channels by extracellular QX314, suggesting that the extracellular pathway bypasses the channel gates, which regulate access through the intracellular pathway (*9*, *13*, *14*).

Intracellular QX314 produced almost no use-dependent block of F1764A channels (Fig. 3C). Because use-dependent block by internal QX314 occurs through open Na^+ channels, this result provides further evidence that F1764A lowered the affinity of the open state for local anesthetics. The

small amount of block that did develop recovered slowly (Fig. 3C), like block of wild-type channels, indicating that F1764A did not alter the escape pathway, so the drug was trapped when the activation or inactivation gates closed.

Our results lead to a model of the local anesthetic receptor site in the pore of the Na^+ channel. Mutations F1764A, Y1771A, and I1760A, which had the strongest effects on use-dependent block, are oriented on the same face of the IVS6 helix (Fig. 4). F1764A and Y1771A reduced open and inactivated channel affinity by one to two orders of magnitude, and F1764A also had a smaller effect on resting channel affinity, suggesting that the native residues at these positions contribute to the free energy of drug binding. F1764 and Y1771 are hydrophobic (*23*), aromatic residues separated by two turns of the S6 helix (Fig. 4), so they are about 11 Å apart. Effective local anesthetics are approximately 10 to 15 Å in length (*24*), with positively charged and hydrophobic moieties at either end that could interact with these residues through hydrophobic (*25*) or π electron (*26*) interactions. Therefore, we propose that F1764 and Y1771 are determinants of the local anesthetic binding site and that substitution of these residues with alanine destabilizes drug binding by reducing the hydrophobicity and aromaticity at these positions. I1760 is oriented on the same face of the helix as F1764 and Y1771 and is therefore well positioned to modulate extracellular access to the local anesthetic binding site. Replacement of the bulky isoleucine residue at position 1760 with alanine allows QX314 to reach the site from the extracellular medium, perhaps by passing directly through the pore from the outside. Thus, I1760 likely corresponds to a narrow region in the pore, just to the extracellular side of the local anesthetic binding site. The mutations I1761A, V1766A, and N1769A increased resting block without altering inactivated state affinity. Because these amino acids are oriented away from the face containing F1764, Y1771, and I1760 (Fig. 4), they may be oriented away from the channel pore. Mutations to alanine at these positions may increase channel sensitivity to drugs through indirect effects on the local anesthetic site, perhaps by partially inducing the inactivated binding site conformation in functionally resting Na^+ channels.

REFERENCES AND NOTES

1. W. A. Catterall, *Physiol. Rev.* **72**, S15 (1992).
2. M. Noda *et al.*, *Nature* **320**, 188 (1986); T. Kayano, N. Noda, V. Flockerzi, H. Takahashi, S. Numa, *FEBS Lett.* **288**, 187 (1988).
3. V. J. Auld *et al.*, *Neuron* **1**, 449 (1988); V. J. Auld *et al.*, *Proc. Natl. Acad. Sci. U.S.A.* **87**, 323 (1990).
4. T. Scheuer *et al.*, *Science* **247**, 854 (1990).
5. J. W. West, T. Scheuer, L. Maechler, W. A. Catterall, *Neuron* **8**, 59 (1992).
6. M. Noda *et al.*, *Nature* **322**, 826 (1986); A. L. Goldin *et al.*, *Proc. Natl. Acad. Sci. U.S.A.* **83**, 7503 (1986).
7. L. L. Isom *et al.*, *Science* **256**, 839 (1992).
8. J. F. Butterworth IV and G. R. Strichartz, *Anesthesiology* **72**, 711 (1990); W. A. Catterall, *Trends Pharmacol. Sci.* **8**, 57 (1987).
9. B. Hille, *J. Gen. Physiol.* **69**, 497 (1977).
10. L. M. Hondeghem and B. G. Katzung, *Biochim. Biophys. Acta.* **427**, 373 (1977); B. P. Bean, C. J. Cohen, R. W. Tsien, *J. Gen. Physiol.* **81**, 613 (1983).
11. C. F. Starmer and K. R. Courtney, *Am. J. Physiol.* **251**, H848 (1986); C. F. Starmer, V. V. Nesterenko, F. R. Gilliam, A. O. Grant, *ibid.* **259**, H626 (1990).
12. D. T. Frazier, T. Narahashi, M. Yamada, *J. Pharm. Exp. Ther.* **171**, 45 (1970).
13. G. R. Strichartz, *J. Gen. Physiol.* **62**, 37 (1973); K. R. Courtney, *ibid.* **195**, 225 (1975).
14. M. Cahalan, *Biophys. J.* **23**, 285 (1978); ——— and W. Almers, *ibid.* **27**, 39 (1979).
15. D. S. Ragsdale, T. Scheuer, W. A. Catterall, *Mol. Pharmacol.* **40**, 756 (1991).
16. J. Striessnig, H. Glossman, W. A. Catterall, *Proc. Natl. Acad. Sci. U.S.A.* **88**, 9203 (1991); W. A. Catterall and J. Striessnig, *Trends Pharmacol. Sci.* **13**, 256 (1992); K. L. Choi, C. Mossman, J. Aubé, G. Yellen, *Neuron* **10**, 533 (1993); G. E. Kirsch, C. C. Shieh, J. A. Drew, D. F. Vener, A. M. Brown, *ibid.* **11**, 503 (1993).
17. D. E. Patton, J. W. West, W. A. Catterall, A. L. Goldin, *Proc. Natl. Acad. Sci. U.S.A.* **89**, 10905 (1992).
18. Experimental conditions for the mutagenesis of IVS6, for its injection, and for the electrophysiological recording of *Xenopus* oocytes have been described [J. C. McPhee *et al.*, *Proc. Natl. Acad. Sci. U.S.A.*, in press]. Abbreviations for the amino acid residues are as follows: A, Ala; C, Cys; D, Asp; E, Glu; F, Phe; G, Gly; H, His; I, Ile; K, Lys; L, Leu; M, Met; N, Asn; P, Pro; Q, Gln; R, Arg; S, Ser; T, Thr; V, Val; W, Trp; and Y, Tyr. Each amino acid is indicated by its one-letter code. The number indicates its position in the chain, and A at the end indicates that alanine has been substituted for the native amino acid. Except where noted by error bars, the data presented in the figures are single examples from three or more experiments that led to the same conclusion.
19. J. S. Richardson, *Adv. Protein Chem.* **34**, 167 (1981); M. Blaber, K. J. Zhang, B. W. Matthews, *Science* **260**, 1637 (1993).
20. W. J. Adelman and Y. Palti, *J. Gen. Physiol.* **54**, 589 (1969); W. K. Chandler and H. Meves, *J. Physiol. (London)* **211**, 707 (1970); J. M. Fox, *Biochim. Biophys. Acta* **426**, 232 (1976); T. Brismar, *J. Physiol. (London)* **270**, 283 (1977); B. Rudy, *ibid.* **283**, 1 (1978); F. N. Quandt, *ibid.* **392**, 563 (1987).
21. J. Z. Yeh and J. Tanguy, *Biophys. J.* **47**, 685 (1985).
22. C. F. Starmer, J. Z. Yeh, J. Tanguy, *ibid.* **49**, 913 (1986).
23. T. P. Hopp and K. R. Woods, *Proc. Natl. Acad. Sci. U.S.A.* **78**, 3824 (1981).
24. K. R. Courtney, *J. Mol. Cell. Cardiol.* **20**, 465 (1988).
25. P. M. Bokesh, C. Post, G. R. Strichartz, *J. Pharm. Exp. Ther.* **237**, 773 (1986); R. S. Sheldon, R. J. Hill, M. Taouis, L. M. Wilson, *Mol. Pharmacol.* **39**, 609 (1991); G. W. Zamponi and R. J. French, *Biophys. J.* **65**, 2335 (1994).
26. L. Heginbotham and R. MacKinnon, *Neuron* **8**, 483 (1992).
27. S. H. Heinemann, H. Terlau, W. Stühmer, K. Imoto, S. Numa, *Nature* **356**, 441 (1992); P. H. Backx, D. T. Yue, J. H. Lawrence, E. Marban, G. F. Tomaselli, *Science* **257**, 248 (1992).

28. Supported by research grants R01-NS15751 and P01-HL44948 from the NIH (to W.A.C.), postdoctoral fellowships from the NIH (to D.S.R. and J.C.M.), and the W. M. Keck Foundation.

1 June 1994; accepted 8 August 1994

Role of a Conserved Retinoic Acid Response Element in Rhombomere Restriction of *Hoxb-1*

Michèle Studer, Heike Pöpperl, Heather Marshall, Atsushi Kuroiwa, Robb Krumlauf*

After activation in mesoderm and neuroectoderm, expression of the *Hoxb-1* gene is progressively restricted to rhombomere (r) 4 in the hindbrain. Analysis of the chick and mouse *Hoxb-1* genes identified positive and negative regulatory regions that cooperate to mediate segment-restricted expression during rhombomere formation. An enhancer generates expression extending into r3 and r5, and a repressor limits this domain to r4. The repressor contains a conserved retinoic acid response element, point mutations in which allow expression to spread into adjacent rhombomeres. Retinoids and their nuclear receptors may therefore participate in sharpening segment-restricted expression of *Hoxb-1* during rhombomere boundary formation.

Rhombomeres are segmental units of organization in the vertebrate hindbrain (*1*). Cell mixing can occur between prospective neighboring segments before rhombomeres become lineage-restricted cellular compartments (*2*). Later, boundaries form between odd- and even-numbered units; however, cells can mix when even- or odd-numbered rhombomeres are grafted adjacent to each other, which suggests that the formation and maintenance of boundaries are dependent on signaling between odd and even segments (*3*). Some of the *Hox* homeobox genes important for regulating axial patterning have limits of expression that coincide with rhombomere boundaries (*4*, *5*). For example, expression of the *Hoxb-1* gene is progressively restricted to r4 in the hindbrain (*4*, *6*–*8*). These patterns of expression, combined with mutational analysis (*9*,

M. Studer, H. Pöpperl, H. Marshall, R. Krumlauf, Lab of Developmental Neurobiology, National Institute for Medical Research, The Ridgeway, Mill Hill, London NW7 1AA, UK.

A. Kuroiwa, Department of Molecular Biology, School of Science, Nagoya University, Chihusa-Ku, Nagoya, Japan 464-01.

*To whom correspondence should be addressed.

Shaded topography of the 12-kilometer-long Asal rift (Djibouti, East Africa). Colors indicate elevations, from −150 meters below (dark blue) to 350 meters above (purple) sea level. The topography results from the tectonic dismemberment over the past 100,000 years of a large central volcano (Fieale) that formed astride the rift zone 300,000 to 100,000 years ago. Reconstruction of this volcano indicates a spreading rate across the rift of 17 to 29 millimeters per year. See page 1677. [Image: J.-B. De Chabalier and J.-P. Avouac]

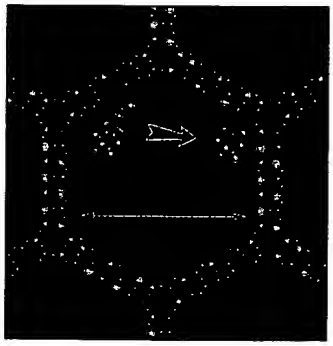

1675
Catalysts at work

1722
Long-range inhibitory neurons in the hippocampus

◪ **Indicates accompanying feature**

■ **SCIENCE (ISSN 0036-8075) is published weekly on Friday, except the last week in December, by the American Association for the Advancement of Science, 1333 H Street, NW, Washington, DC 20005.** Second-class postage (publication No. 484460) paid at Washington, DC, and additional mailing offices.

Domestic individual membership and subscription (51 issues): $92 ($50 allocated to subscription). Domestic institutional subscription (51 issues): $215. Foreign postage extra: Mexico, Caribbean (surface mail) $50; other countries (air assist delivery) $95. First class, airmail, student and emeritus rates on request. Canadian rates with GST available upon request, GST #1254 88122. **Printed in the U.S.A.**

Change of address: allow 6 weeks, giving old and new addresses and 11-digit account number. **Postmaster:** Send change of address to *Science*, P.O. Box 2033, Marion, OH 43305-2033. **Single copy sales:** $6.00 per issue prepaid includes surface postage; Guide to Biotechnology Products and Instruments, $20. Bulk rates on request. **Authorization to photocopy** material for internal or personal use under circumstances not falling within the fair use provisions of the Copyright Act is granted by AAAS to libraries and other users registered with the Copyright Clearance Center (CCC) Transactional Reporting Service, provided that the base fee of $1 per copy plus $0.10 per page is paid directly to CCC, 27 Congress Street, Salem, MA 01970. The identification code for *Science* is 0036-8075/83 $1 + .10. *Science* is indexed in the *Reader's Guide to Periodical Literature* and in several specialized indexes.

This Page is Inserted by IFW Indexing and Scanning Operations and is not part of the Official Record

BEST AVAILABLE IMAGES

Defective images within this document are accurate representations of the original documents submitted by the applicant.

Defects in the images include but are not limited to the items checked:

- ☐ **BLACK BORDERS**
- ☐ **IMAGE CUT OFF AT TOP, BOTTOM OR SIDES**
- ☐ **FADED TEXT OR DRAWING**
- ☐ **BLURRED OR ILLEGIBLE TEXT OR DRAWING**
- ☐ **SKEWED/SLANTED IMAGES**
- ☐ **COLOR OR BLACK AND WHITE PHOTOGRAPHS**
- ☐ **GRAY SCALE DOCUMENTS**
- ☑ **LINES OR MARKS ON ORIGINAL DOCUMENT**
- ☐ **REFERENCE(S) OR EXHIBIT(S) SUBMITTED ARE POOR QUALITY**
- ☐ **OTHER:** _____

IMAGES ARE BEST AVAILABLE COPY.
As rescanning these documents will not correct the image problems checked, please do not report these problems to the IFW Image Problem Mailbox.